Journal of Fluids and Structures (1999) **13,** 309–338
Article No.: jfls.1999.0205 available online at http://www.idealibrary.com on IDEAL

FLUID BEHAVIOUR OF SIDE-BY-SIDE CIRCULAR CYLINDERS IN STEADY CROSS-FLOW

D. Sumner†, S. S. T. Wong, S. J. Price and M. P. Païdoussis

Department of Mechanical Engineering, McGill University, Montréal, Québec, Canada

(Received 18 December 1997 and in revised form 30 October 1998)

The flow field for two and three circular cylinders of equal diameter D arranged in a side-by-side configuration in steady cross-flow was investigated using flow visualization, hot-film anemometry and particle image velocimetry (PIV), for centre-to-centre pitch ratios from $T/D = 1{\cdot}0$ to $6{\cdot}0$, and Reynolds numbers from $\mathrm{Re} = 500$ to 3000. For two-cylinder arrangements, three basic flow patterns were observed: single bluff-body vortex shedding at small T/D, biased flow with synchronized vortex shedding at intermediate T/D, and symmetric flow with synchronized vortex shedding at larger T/D. For three-cylinder arrangements, either single bluff-body behaviour or an asymmetric biased flow pattern could be observed at small T/D, whereas a symmetric-biased flow pattern was found at intermediate T/D. Instantaneous representations of the in-plane vorticity field obtained from the PIV technique revealed some variation in these basic flow patterns at given T/D and Re.

1. INTRODUCTION

When immersed in steady cross-flow of velocity U, two circular cylinders of equal diameter D, arranged in a side-by-side configuration [Figure 1(a)], are known to exhibit an asymmetrical flow pattern for intermediate values of the centre-to-centre transverse pitch ratio T/D separating the two cylinders (Spivack 1946; Hori 1959; Ishigai *et al.* 1972; Bearman & Wadcock 1973; Kamemoto 1976; Kiya *et al.* 1980; Williamson 1985; Jendrzejczyk & Chen 1986; Kim & Durbin 1988; Le Gal *et al.* 1990; Sumner *et al.* 1997). The asymmetrical flow pattern is characterized by a narrow near-wake region behind one of the cylinders, a wide near-wake behind the other cylinder, and two dominant vortex-shedding frequencies (which may be expressed in nondimensional form in terms of the Strouhal number, $\mathrm{St} = f_s D/U$, where f_s is the vortex-shedding frequency). In some cases, the biased flow pattern switches intermittently from being directed towards one cylinder to the other, and the flow pattern is termed bistable (Bearman & Wadcock 1973; Kim & Durbin 1988). This biased flow pattern is observed in the range of $1{\cdot}2 < T/D < 2{\cdot}2$ approximately, and is nominally independent of the Reynolds number, Re (based on the cylinder diameter D and the approach velocity U). At smaller pitch ratios, $T/D < 1{\cdot}2$, the two cylinders behave in a similar fashion to a single bluff body, whereas at higher pitch ratios, $T/D > 2{\cdot}2$, the flow field regains its symmetry. Existing experimental investigations of two side-by-side circular cylinders are summarized in Table 1(a).

Side-by-side configurations of *three* circular cylinders of equal diameter exhibit different behaviour, but have received less attention (Eastop & Turner 1982; Kumada *et al.* 1984; Sumner *et al.* 1997). The relevant studies are summarized in Table 1(b). Flow patterns include single bluff-body behaviour and asymmetric biased flow at small pitch ratios, and symmetric biased flow about the central cylinder at intermediate pitch ratios.

†Presently at University of Saskatchewan, Saskatoon, Saskatchewan, Canada.

0889–9746/99/040309 + 30 $30.00

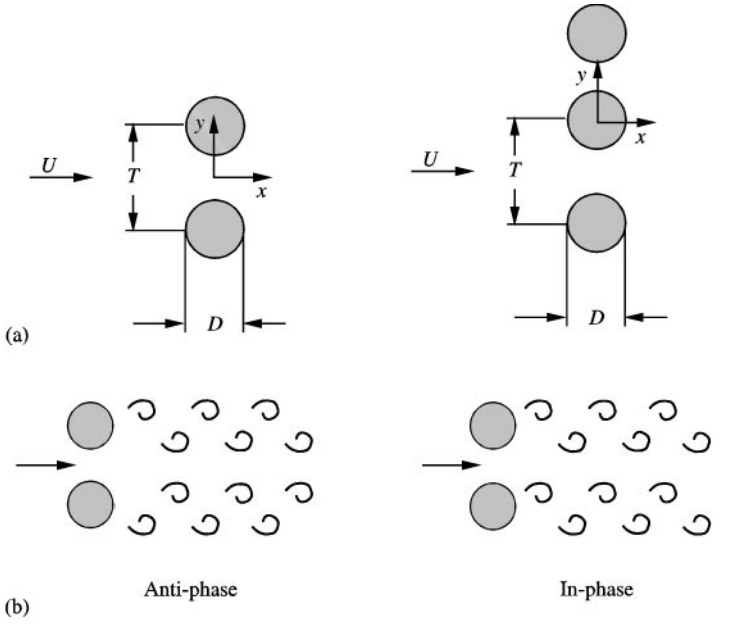

Figure 1. (a) Nomenclature for two and three side-by-side circular cylinders of equal diameter in steady cross-flow. (b) Anti-phase and in-phase vortex street synchronization.

The existence of two or more simultaneous, side-by-side vortex-shedding processes and vortex streets for this arrangement of cylinders leads to complex vortex street interaction in the combined wake of the bodies (Le Gal *et al.* 1990; Peschard & Le Gal 1996). Typically, two vortex streets are synchronized in an anti-phase fashion [Figure 1(b)], in which vortices are shed simultaneously on both sides of the gap between two of the cylinders (Williamson 1985). Alternatively, in-phase vortex-shedding synchronization may be observed.

Multiple cylinders arranged side-by-side in a single row have also been examined (Ishigai & Nishikawa 1975; Moretti & Cheng 1987; Cheng & Moretti 1988; Zdravkovich & Stonebanks 1990; Le Gal *et al.* 1996). They are noted for irregular flow patterns involving the coalescence and deflection of any number of the gap-flow jets, particularly for $T/D < 2$. The gap flows may also intermittently switch direction, and different groups of jets may intermittently coalesce. These flows have been termed "metastable" (Zdravkovich & Stonebanks 1990). These features of the flow are similar to those observed for the two- and three-cylinder arrangements.

In this study, the dynamics of the flow about two and three circular cylinders of equal diameter arranged in a side-by-side configuration is examined using flow visualization, hot-film anemometry, and particle image velocimetry (PIV), for Reynolds numbers ranging from 500 to 3000. Use of the PIV techinque in particular has enabled some new insight to be obtained into the complexity of the flow field as the pitch ratio is varied.

In many engineering applications, such as offshore structures, heat exchangers, power transmission lines, and chimneys, multiple cylindrical structures are often found in close proximity. Study of the fluid dynamics of side-by-side cylinders should then afford an improved understanding or vortex-shedding-induced vibration and fluid–structure interaction for such multiple bluff-body configurations.

TABLE 1(a)

Experimental investigations of two side-by-side circular cylinders of equal diameter in steady cross-flow. Measured quantities: (a) Strouhal number, (b) mean surface pressure distribution, (c) base pressure, (d) mean drag coefficient, (e) mean lift coefficient, (f) r.m.s. drag coefficient, (g) r.m.s lift coefficient, (h) time-averaged velocity profiles, (i) velocity field, (j) vorticity field, (k) spanwise coherence or correlation measurements. Abbreviations: FV = flow visualization; CTA = constant temperature anemometry; PIV = particle image velocimetry. Blockage ratio based on total blockage for two cylinders

Researchers	Re	T/D	Facility	Technique	Aspect ratio	Blockage ratio	Turbulence intensity	Measurements
Bearman & Wadcock (1973)	25 000	1·0–7·0	Wind tunnel	FV	31	4%	0·2%	a,b,c,d,e,k
Hori (1959)	200–12 000	1·2–3·0	Wind tunnel	CTA, pressure	120	1%	0·03%	a,b,c,h
Ishigai *et al.* (1972)	1500–15 000	1·25–3·0	Wind tunnel	FV, CTA, pressure	11	18%	not given	a
Jendrzejczyk & Chen (1986)	$15\,000$–$1{\cdot}5 \times 10^5$	1·35,2·7	Wind tunnel	Force balance	12	17%	1·0–11·0%	a,f,g
Kamemoto (1976)	662	1·5–3·0	Towing tank	FV, CTA	75	3%	–	a
Kamemoto (1976)	30 000	1·0–3·0	Wind tunnel	CTA	5	13%	not given	a
Kim & Durbin (1988)	3300	1·0–3·0	Wind tunnel	FV, CTA, pressure	27	3%	0·2%	a,c,i
Kiya *et al.* (1980)	15 800	1·0–5·5	Wind tunnel	CTA	21	2%	0·8%	a
Kwon *et al.* (1996)	17 800	1·1–3·0	Water channel	PIV	11	2%	2·5%	i
Le Gal *et al.* (1990)	110	1·0–7·5	Water tunnel	FV	50	4%	1·0%	–
Peschard & Le Gal (1996)	90–150	1·0–6·0	Water tunnel	FV	7	not given	1.0%	–
Spivack (1946)	5000–93 000	1·0–6·0	Wind tunnel	CTA	39	5%	0·02%	a,h
Williamson (1985)	50–150	1·0–6·0	Wind tunnel	FV	279	1%	not given	a
Williamson (1985)	200	1·0–6·0	Water tunnel	FV	13	8%	not given	a
Zdravkovich & Pidden (1977)	60 000	1·0–3·0	Wind tunnel	Force balance	33	5%	0·1%	d,e
Current study	500–3000	1·0–6·0	Water tunnel	FV, CTA	16	13%	0·5%	a
Current study	1200–3000	1·0–3·0	Towing tank	PIV	27	7%	–	i,j

TABLE 1(b)

Summary of experimental investigations of three side-by-side circular cylinders of equal diameter in steady cross-flow. Measured quantities: (a) Strouhal number, (b) mean surface pressure distribution, (c) base pressure, (d) mean drag coefficient, (e) mean lift coefficient, (f) separation angle, (g) time averaged velocity profiles, (h) velocity field, (i) vorticity field. Abbreviations: FV = flow visualization; CTA = constant temperature anemometry; PIV = particle image velocimetry. Blockage ratio based on total blockage for three cyclinders

Researchers	Re	T/D	Facility	Technique	Aspect ratio	Blockage ratio	Turbulence intensity	Measurements
Eastop & Turner (1982)	45 000–111 000	1·2–2·6	Wind tunnel	CTA, pressure	14	21%	0·7%	a,c,d,f
Kumada *et al.* (1984)	10 000–32 000	1·0–3·75	Wind tunnel	FV, CTA, pressure	15	20%	0·2%	a,b,c,d,e,g
Current study	500–3000	1·0–3·0	Water tunnel	FV, CTA	16	19%	0·5%	a
Current study	1200–3000	1·0–1·5	Towing tank	PIV	27	11%	–	h,i

2. EXPERIMENTAL APPARATUS

2.1. Flow Visualization and Hot-Film Anemometry

The flow visualization and hot-film anemometry experiments were conducted in a closed-loop water tunnel with a working section of 254 mm × 254 mm cross-section, and a longitudinal freestream turbulence intensity of 0·5% (Figure 2). The cylinder models were

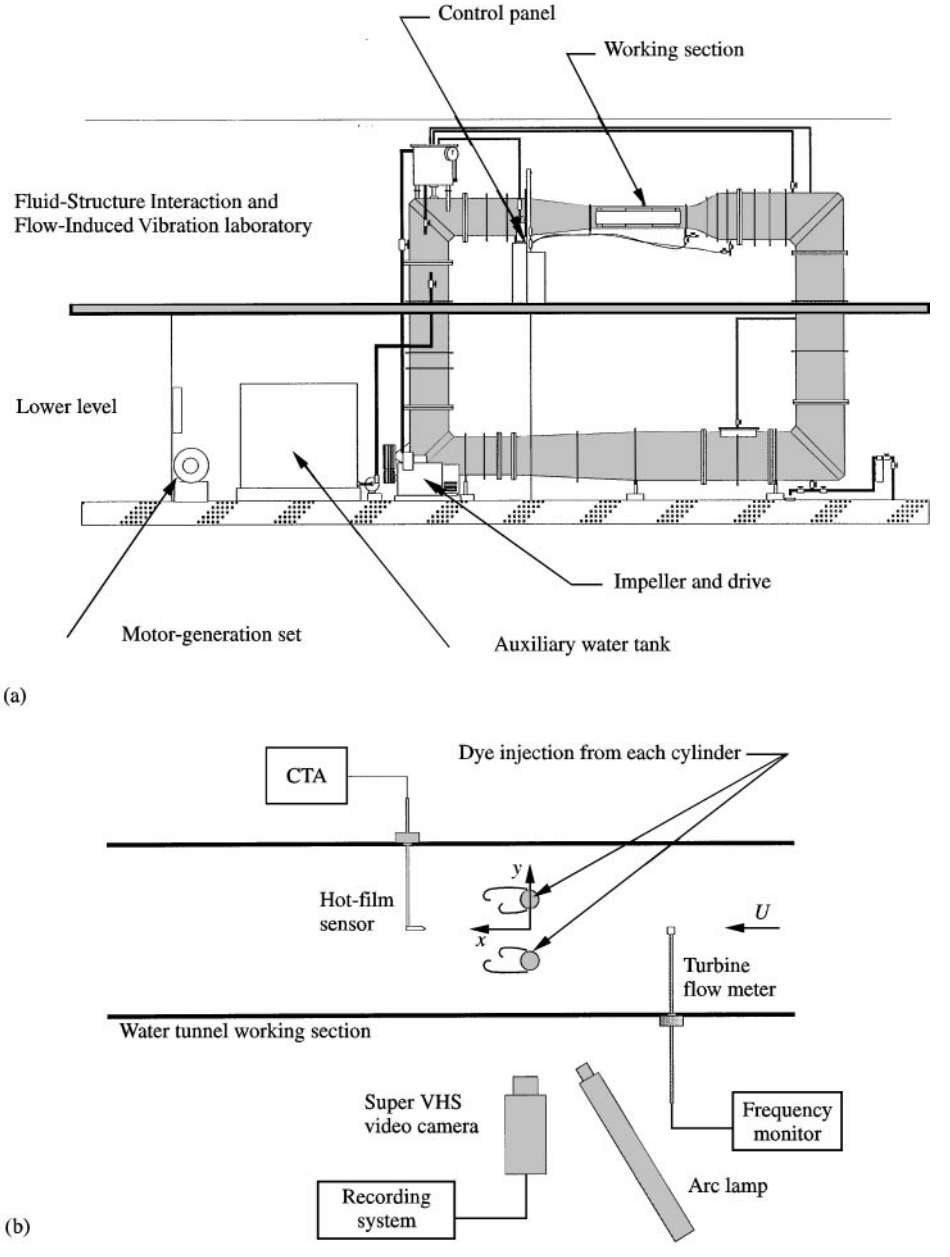

Figure 2. (a) Closed-loop water tunnel. (b) Experimental set-up in the water tunnel working section.

constructed of Plexiglas ($D = 16$ mm), and had aspect ratios of 16 and solid blockage ratios (per cylinder) of 6·3%. No end-plates were fitted to the cylinders in the water tunnel experiments. Each cylinder had two dye injection ports of 0·8 mm diameter located at mid-span and near the points of boundary layer separation. The flow velocity ranged from $U = 30$ to 190 mm/s. The experiments conducted in the water tunnel examined two-cylinder configurations with T/D varied from 1·0 to 6·0, and three-cylinder configurations with $T/D = 1{\cdot}0$ to 3·0, with the spacing incremented by $0{\cdot}5D$ in each case. The Reynolds number for the flow visulaization ranged from Re = 500 to 1500, and that for the hot-film anemometry from Re = 500 to 3000.

For flow visualization, fluorescein and rhodamine dyes were injected into the near-wake regions of the cylinders. The dye was illuminated using a narrow sheet of light from a xenon arc lamp, and the fluid motion was captured with a JVC KY-25U Super-VHS video camera, as shown in Figure 2(b). Digital images were then acquired from the individual video frames using a personal computer with a video-input card, and enhanced for analysis using Adobe Photoshop software.

A TSI model 1269 single-component hot-film sensor was used to obtain measurements of the vortex-shedding frequency in the wake of the multiple cylinder configurations. The sampling rate was typically 20 Hz, and the sampling time ranged from 5 to 10 min. For vortex-shedding frequencies of the order of 0·5–2 Hz, the sampling time corresponded to between 150 and 1200 vortex-shedding periods. The probe was typically located between two and five diameters downstream of the cylinders, and at a range of cross-stream positions.

2.2 Particle Image Velocimetry (PIV)

The particle image velocimetry (PIV) experiments were conducted in a newly designed and constructed water towing tank (Figure 3) of 0·76 m × 0·76 m cross-section and 3·05 m

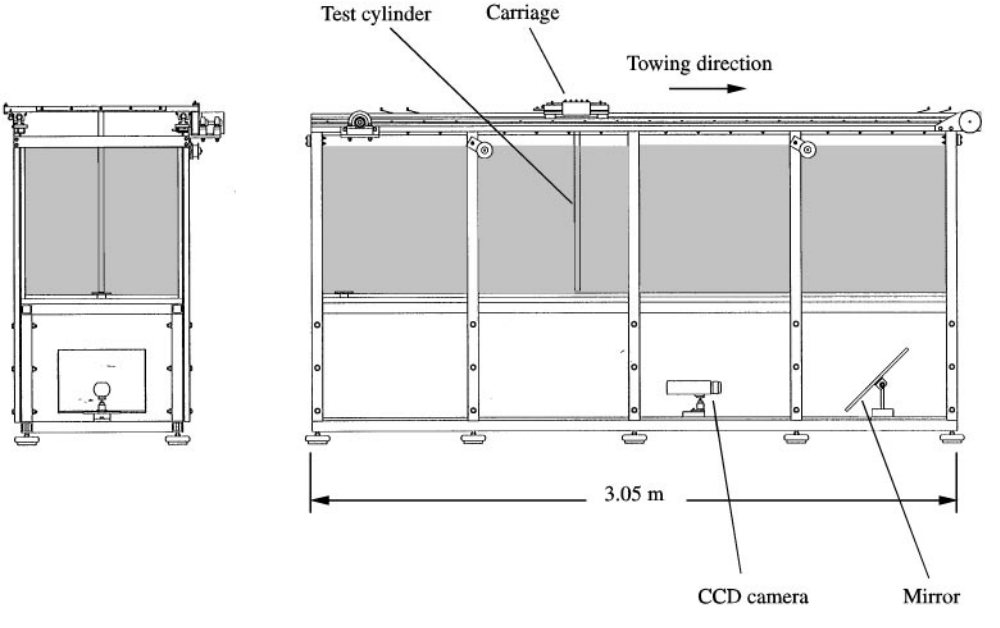

Figure 3. Main water towing tank facility, shown with a single circular cylinder (without an end-plate fitted) rigidly suspended vertically from the carriage.

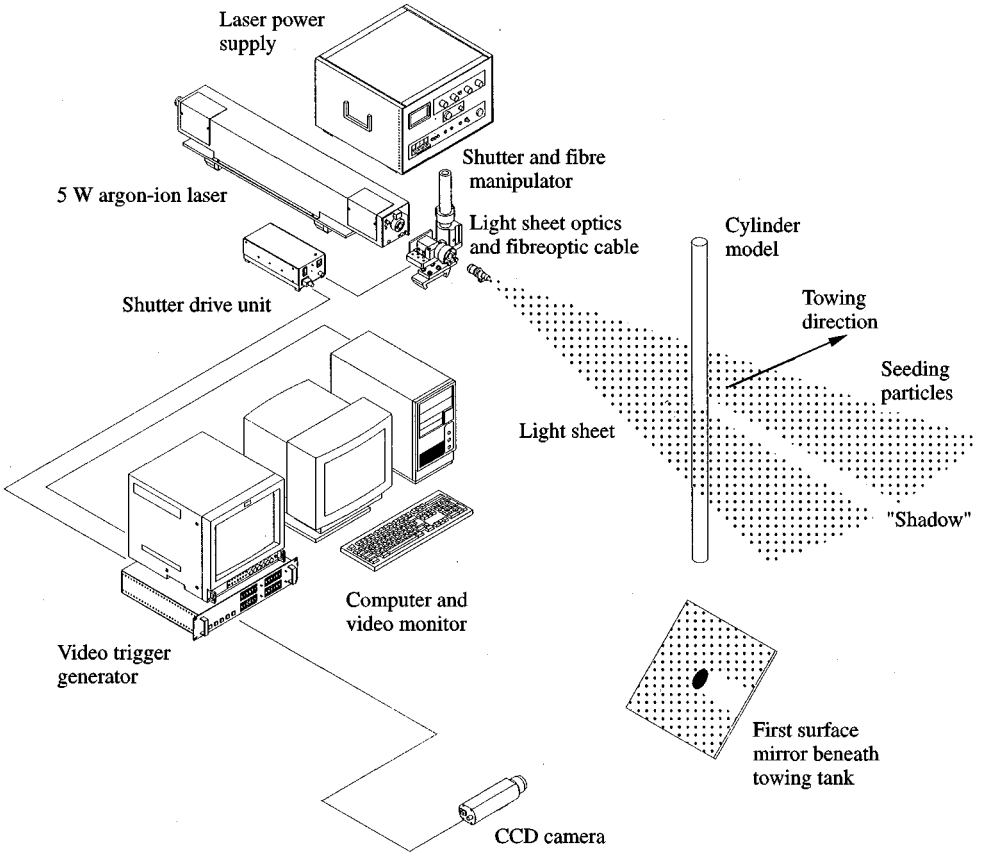

Figure 4. Components of the particle image velocimetry (PIV) system.

length. Each cylinder was constructed of stainless steel ($D = 25{\cdot}4$ mm) and had an aspect ratio of 27. The solid blockage ratio was 7% for the two-cylinder configurations and 10·5% for the three-cylinder configurations. A single end-plate made from Plexiglas was fitted to the multiple-cylinder configuration at the free end near the bottom of the tank, based on the optimized design of Szepessy (1993) for a single cylinder. The towing velocity ranged from $U = 50$ to 120 mm/s, yielding Reynolds numbers from $\mathrm{Re} = 1300$ to 2900. The PIV experiments examined two-cylinder configurations of $T/D = 1{\cdot}0$, 1·125, 1·5, 1·75, 2·0, 2·5 and 3·0, and three-cylinder configurations of $T/D = 1{\cdot}0$, 1·125, 1·25 and 1·5.

For the application of PIV (Figure 4), the water was seeded with irregularly shaped, nearly neutrally buoyant particles, of 100–300 μm in size. A section of the flow was illuminated with a pulsed light sheet generated by a 5 W argon-ion laser and a mechanical shutter, and successive pairs of single-exposed digital particle images (each of 512×480 pixels) were acquired with a Dantec Double Image 700 CCD camera and frame grabber (a different system from that used for the flow visualization experiments). The horizontal image magnification was of the order of 0·3 mm/pixel, and each image covered an area of approximately 150×150 mm (6×6 cylinder diameters) within the flow field. The image exposure time was typically 6 ms, and the time between single-exposed images constituting a pair was typically 4 ms. In the 10 ms time difference between the images comprising a pair, a particle moving at the freestream velocity of 75 mm/s would cover 2·5 pixels (0·75 mm or 0·03 diameters).

As shown in Figures 3 and 4, the camera was mounted in a fixed position beneath the towing tank, and images were acquired, with the aid of a mirror, through the glass bottom of the towing tank and the Plexiglas end-plate. The light sheet was located at the centre-span of the cylinder, midway between the free surface of the water and the end-plate. End effects due to the free surface and the end-plate were found to be confined to spanwise distances of approximately 7 diameters, so that the central portion of the span of 13 diameters was subject to nominally two-dimensional flow conditions.

Dantec FlowGrabber digital PIV software employing the cross-correlation algorithm of Willert & Gharib (1991) was used to compute the raw displacement vector field from the particle image data, using an interrogation window of 32×32 pixels (approximately 10×10 mm, or $0{\cdot}3 \times 0{\cdot}3$ cylinder diameters) with 75% overlap. The size of the interrogation window effectively limits the minimum size of the vortex structures which can be identified in these experiments to approximately 0·3 cylinder diameters. Software developed in-house was then used to compute the in-plane velocity vector field (57×57 vectors) and vorticity field (55×55 points) at a spacing of about 2·6 mm (or 0·1 cylinder diameters).

The time between successive pairs (or sets of vorticity data) was $\Delta t = 0{\cdot}2$ s. This time interval between successive vorticity fields may be expressed as a fraction of the vortex-shedding period T_s, determined from published vortex-shedding frequency data (from references in Table 1), where $\Delta t/T_s = \Delta t^*\mathrm{St}$ (in which $\Delta t^* = \Delta t U/D$). In these experiments, this time difference between sets of vorticity data corresponds to 0·04 to 0·24 vortex shedding periods, depending on the configuration of the cylinders, the Reynolds number, and the shedding frequency. Images were acquired near the end of a towing run of about 2·5 m, corresponding to a nondimensional elapsed time from the start of towing of $t^* = tU/D = 98$ at $\mathrm{Re} = 1900$ (for elapsed time t from the start of motion).

For each configuration, up to 10 different PIV experiments were conducted, with each yielding eight vorticity fields. Since vorticity fields were acquired at time intervals of $0{\cdot}04T_s$ to $0{\cdot}24T_s$, sufficient information would have been acquired to represent the fluid behaviour of an individual shed vortex over a complete period. A time history of the nondimensional, instantaneous, in-plane vorticity field, $\omega_z D/U$, was determined from a single towing of the cylinders, however, no ensemble averaging or phase averaging of data from successive runs was undertaken (nor were these techniques possible with the given experimental set-up). In most cases, there was a good correspondence between the dye-injection streakline flow visualization images and the instantaneous PIV vorticity data. By applying known displacements to a digitized particle image using Adobe Photoshop software, the measurement uncertainty of the velocity and vorticity data could be assessed; the measurement uncertainty of the vorticity was conservatively estimated at 10%. In the figures and results to be presented in what follows, the smallest magnitude contour of vorticity plotted was typically 10–20% of the maximum vorticity in the flow field.

Given that the cylinders were constructed of stainless steel, it was not possible for the entire flow field to be illuminated with the light sheet. The light source was placed in such a way to illuminate the combined wake region of the cylinders, with the "shadow" (shown schematically in Figure 4) created by the stainless-steel cylinders oriented in the cross-stream direction and in the direction of towing. The direction of the light sheet is shown for reference in Figure 8(a).

3. RESULTS AND DISCUSSION

The Strouhal number data obtained from the hot-film anemometry results are summarized for two- and three-cylinder configurations in Figure 5(a) and 5(b), respectively, and compared to previously published data (obtained at higher Reynolds numbers, as summarized

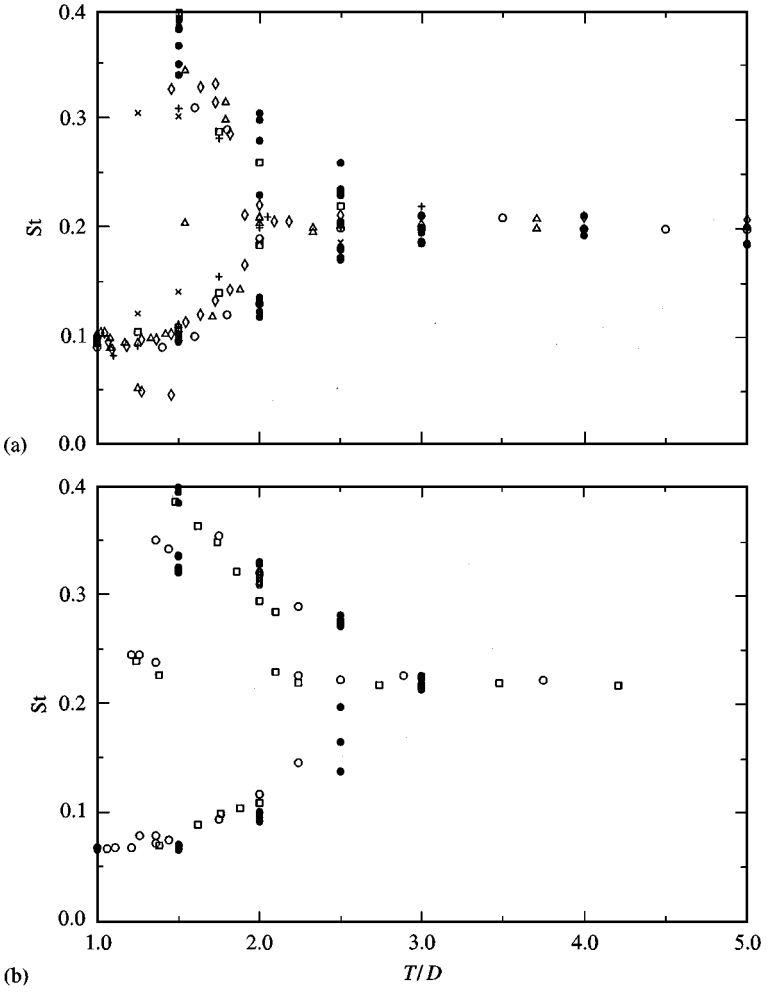

Figure 5. Strouhal number data as a function of transverse pitch ratio. (a) Two side-by-side circular cylinders: ○ Kiya *et al.* (1980); □ Kim & Durbin (1988); Δ, Bearman & Wadcock (1973); ◇, Spivack (1946); ×, Ishigai *et al.* (1972); +, Kamemoto (1976); ●, current study. (b) Three side-by-side circular cylinders: ○, Kumada *et al.* (1984); □, Eastop & Turner (1982); ●, current study.

in Table 1). In general, the Strouhal number data obtained in the present study, for both two and three side-by-side cylinders, agree well with previously published data obtained at higher Reynolds numbers. This agreement shows that the fluid dynamics of the side-by-side arrangement, at least in terms of the Strouhal number, is quite insensitive to changes in Reynolds number, for at least $500 < \mathrm{Re} < 111\,000$. However, some disagreement is noted for both the two- and three-cylinder configurations at $T/D = 2{\cdot}5$, with the two-Strouhal-number regime persisting to higher T/D than in the other studies. This difference, as well as the Strouhal number data in general, are discussed further in the following sections.

Sample power spectra (from a single velocity time history, with no averaging) for the wake behind two cylinders are presented in Figure 6. At pitch ratios of $T/D = 1{\cdot}5$ and $2{\cdot}0$, shown in Figure 6(b, c), two dominant frequencies are measured. These two frequencies signify the existence of the biased flow regime, and correspond to two different vortex-shedding processes, caused by the deflection of the gap flow towards one of the two

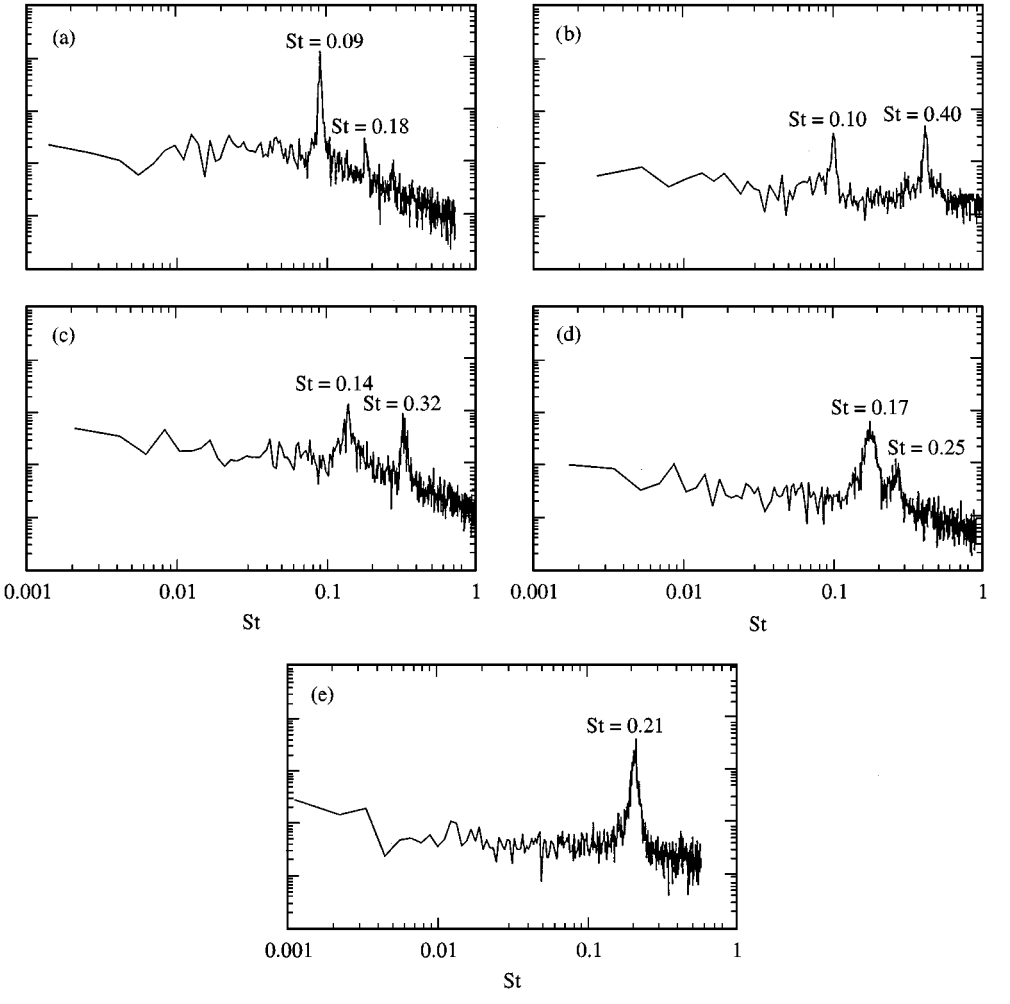

Figure 6. Representative power spectra for two side-by-side circular cylinders in steady cross-flow: (a) $T/D = 1{\cdot}0$, Re = 1700; (b) $T/D = 1{\cdot}5$, Re = 1850; (c) $T/D = 2{\cdot}0$, Re = 1200; (d) $T/D = 2{\cdot}5$, Re = 1450; (e) $T/D = 3{\cdot}0$, Re = 2200. Vertical scale is arbitrary, but the same for each spectrum. Measurement location typically 2–3 diameters downstream and 1–2 diameters from the centreline (depending on configuration).

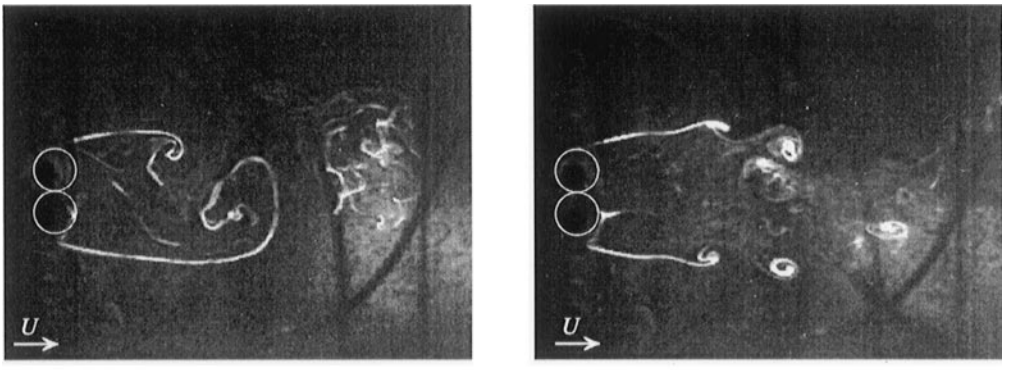

Figure 7. Flow visualization of two side-by-side circular cylinders in steady cross-flow, with $T/D = 1{\cdot}0$: (a) alternate vortex shedding, Re = 1320; (b) irregular vortex shedding, Re = 820.

cylinders (as discussed subsequently in this paper). Two frequencies are also found at $T/D = 2{\cdot}5$ [see Figure 6(d)], although a biased flow pattern is not readily detectable in the flow visualization and PIV results.

3.1. Two and Three Circular Cylinders in Contact, $T/D = 1{\cdot}0$

When two or three side-by-side circular cylinders are in contact with one another, at a pitch ratio of $T/D = 1{\cdot}0$, single bluff-body alternate vortex formation behaviour is observed, and a single vortex street is visible in the wake. The frequency of vortex shedding in both configurations is lower than that of a single circular cylinder, as can be seen in Figure 5, and reflects the increased spacing of two diameters between the two free shear layers when the cylinders are in contact. A strong, low-frequency peak is seen in the power spectrum of Figure 6(a), with a smaller peak found at twice the frequency corresponding to shedding from both shear layers. The single bluff-body behaviour is seen in the flow visualization results of Figure 7 for the two-cylinder configuration, and in the PIV results of Figure 8 for both the two- and three-cylinder configurations. Also shown in Figure 8(a) is the orientation of the laser light sheet.

The PIV results show that the vortices are irregular in shape, and that the shear layers tend to break up easily into small concentrations of vorticity (Wei & Smith 1986; Chyu & Rockwell 1996), perhaps related to Kelvin–Helmholtz instabilities, that seem at times to combine into larger vortices during the process of formation and shedding [Figure 8(b)]. Such behaviour could also be observed, to some extent, in the dye visualization experiments in the water tunnel, although it is not seen in Figure 7.

In the water tunnel, the regular vortex shedding, as seen in Figure 7(a), was often supplanted for periods of time by irregular or symmetric vortex shedding, the latter shown in Figure 7(b). Furthermore, the more disorganized nature of the vorticity field from the PIV experiments reflects a less-intense vortex formation process for the case of the cylinders in contact, seen in the flow visualization videos. The PIV results also revealed a range of alternate shedding for two and three cylinders in contact. Variation was observed (qualitatively) in the vortex formation length, for example, with vortices occasionally forming very close to the cylinders or further into the near-wake. Such variation may reflect different "modes" of fluid behaviour or, more simply, different stages in the shedding cycle (for which a complete cycle could not be captured with the PIV system used in this study). The PIV results also showed some variation in the cross-stream extent of the formed vortex, which may or may not extend across the wake centreline; such variations in behaviour were also observed in the flow visualization results.

3.2. Two Side-by-Side Circular Cylinders with Small T/D

At small pitch ratios, for $1{\cdot}0 < T/D < 1{\cdot}2$, the single bluff-body behaviour noted for $T/D = 1{\cdot}0$ becomes slightly modified. Flow through the gap behaves in a similar fashion to base-bleed (Bearman & Wadcock 1973). Higher-momentum fluid, which enters through the gap, increases the base pressure, reduces the drag of both cylinders, and increases the streamwise extent of the vortex formation region. The vortex-shedding frequency, however, tends to remain close to that observed for $T/D = 1{\cdot}0$, as noted in previously published data compiled in Figure 5(a). Furthermore, a single vortex street is still observed in the combined wake of the two cylinders, and shedding occurs only from the outside shear layers.

This range of transverse pitch ratio was investigated with PIV only, at a single pitch ratio of $T/D = 1{\cdot}125$ (Figure 9). Three types of behaviour were observed in these experiments.

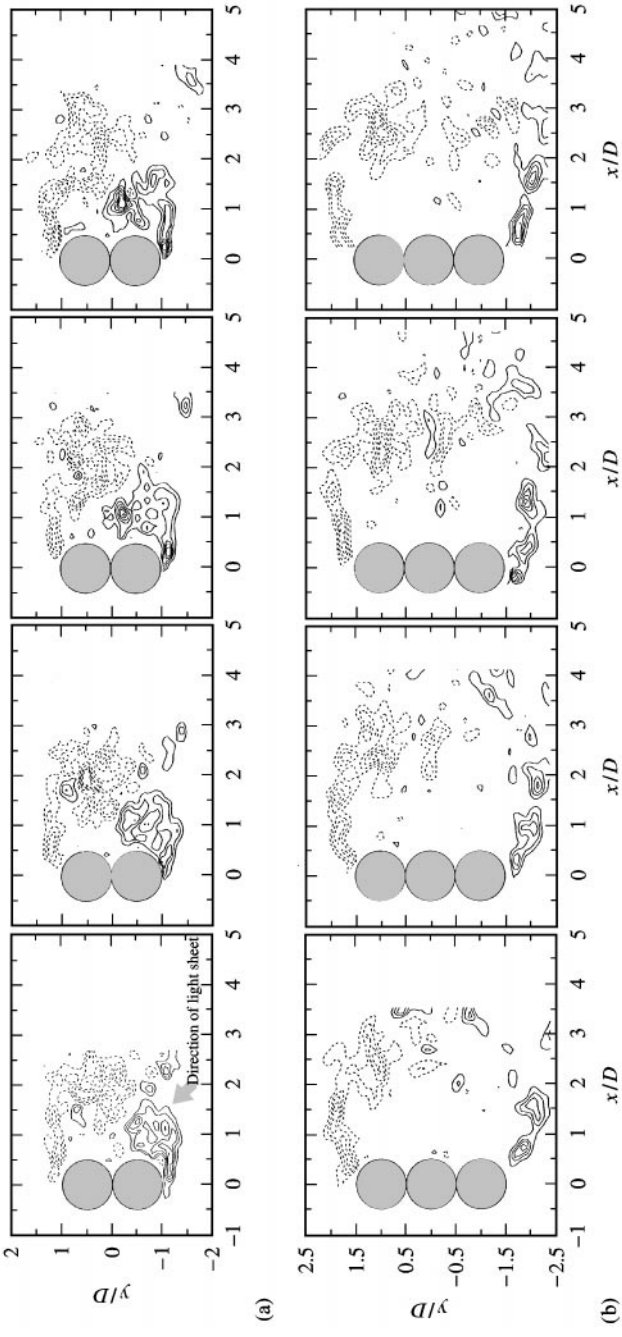

Figure 8. Nondimensional, instantaneous, in-plane vorticity field for side-by-side circular cylinders of equal diameter in steady cross-flow (from left to right), with $T/D = 1{\cdot}0$: (a) two cylinders, Re = 1300, $\Delta t^* = 0{\cdot}4$, $\Delta t/T_s = 0{\cdot}04$; (b) three cylinders, Re = 1900, $\Delta t^* = 0{\cdot}6$, $\Delta t/T_s = 0{\cdot}04$. Minimum vorticity contour magnitude of 1·5, vorticity contour magnitude increment of 1·5. Solid lines represent positive (CCW) vorticity; dashed lines represent negative (CW) vorticity. The direction of the laser light sheet is shown in the first vorticity field in (a).

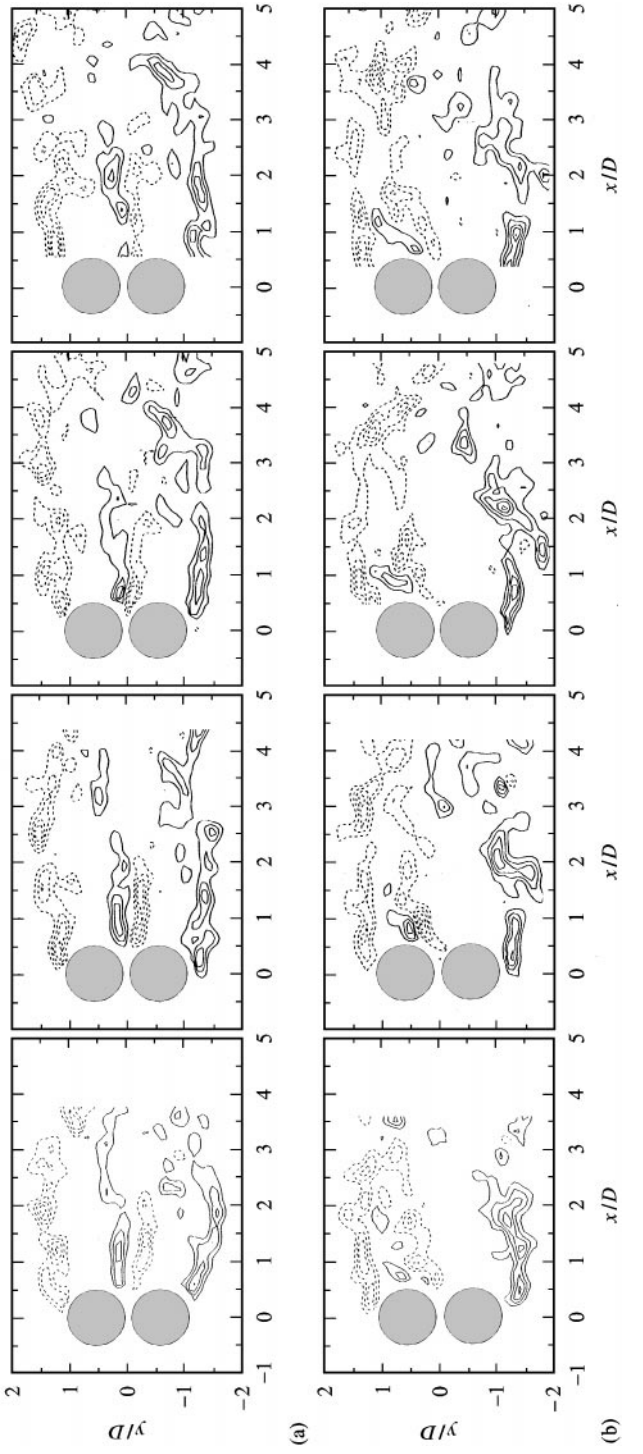

Figure 9. Nondimensional, instantaneous, in-plane vorticity field for two side-by-side circular cylinders of equal diameter in steady cross-flow (from left to right), with $T/D = 1{\cdot}125$, $\mathrm{Re} = 1900$, $\Delta t^* = 0{\cdot}6$, $\Delta t/T_s = 0{\cdot}05$: (a) gap flow remains unbiased and directed along near-wake centreline from the base region; (b) gap flow biased towards the vortex being formed. Minimum vorticity contour magnitude of 1·5; vorticity contour magnitude increment of 1·5. Dashed lines represent negative (CW) vorticity.

Figure 9(a) shows the first flow pattern with a symmetrical near-wake, formation of a single vortex street, and a gap-flow oriented parallel to the flow axis. The gap flow is denoted by the parallel shear layers that persist until about $x/D = 2{\cdot}0$, where the two shear layers end without vortex formation. Formation of a Kármán vortex is shown in the fourth set of vorticity data in Figure 9(a), forming from the outer shear layer of the lower cylinder (in the figure; for in the experiment both cylinders are in fact vertical). Figure 9(b) shows the second flow pattern, with an asymmetrical near-wake region with a deflected or biased gap-flow, although a single vortex street still seems to form further downstream. This second flow pattern was that most commonly observed. A third flow pattern, not shown in Figure 9, showed no significant gap flow (at least in terms of appreciable vorticity). Each flow pattern, however, exhibited single bluff-body behaviour, as shown in Figure 9(a, b).

For the case of deflected flow, this was always observed to favour the uppermost cylinder; however this may have been caused by minor misalignment of the two cylinders. Although the first flow pattern could be considered to correspond to the expected fluid behaviour, the second, asymmetric flow pattern was more commonly observed. The existence of the second flow pattern suggests that it could represent a transition between the single bluff-body flow pattern and the biased flow pattern obtained at greater T/D.

3.3. Two Side-by-Side Circular Cylinders with Intermediate T/D

The biased flow pattern for two cylinders is found at intermediate pitch ratios, from $T/D = 1{\cdot}2$ to $2{\cdot}2$, although there is some evidence to suggest that it may extend to slightly higher or lower T/D, depending on the experimental conditions and the Reynolds number. The cylinder towards which the flow is biased has a narrow near-wake and higher-frequency vortex shedding, while the other cylinder has a wider near-wake and lower-frequency vortex shedding. This biased flow pattern is shown in the flow visualization results in Figure 10 for $T/D = 1{\cdot}5$ and $2{\cdot}0$, and in the velocity, streamline, and vorticity results from PIV in Figure 11 for $T/D = 1{\cdot}25$, $1{\cdot}5$, $1{\cdot}75$ and $2{\cdot}0$.

In both the velocity field and streamline field data, it is noted that there is a region behind the cylinders with no data; this is region of the shadow created by the stainless-steel cylinders in the laser light sheet [source shown in Fig 8(a)]. In Figure 11, streamlines are

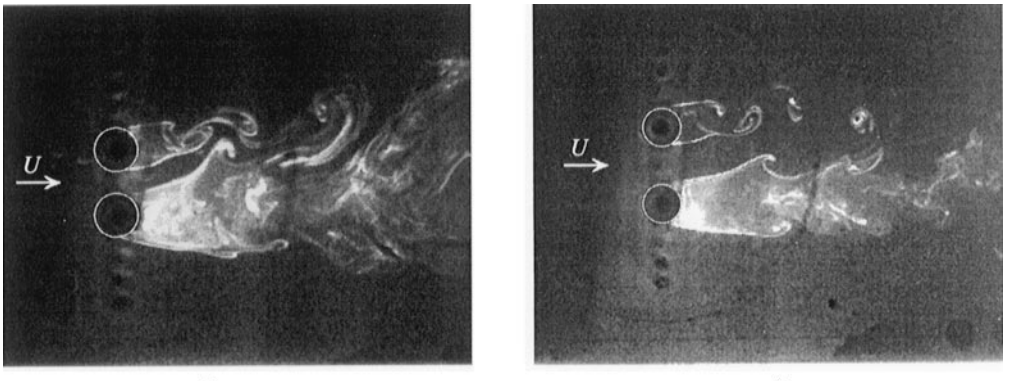

Figure 10. Flow visualization of two side-by-side circular cylinders in steady cross-flow, with a biased flow pattern, for Re = 1000–3000: (a) $T/D = 1{\cdot}5$; (b) $T/D = 2{\cdot}0$.

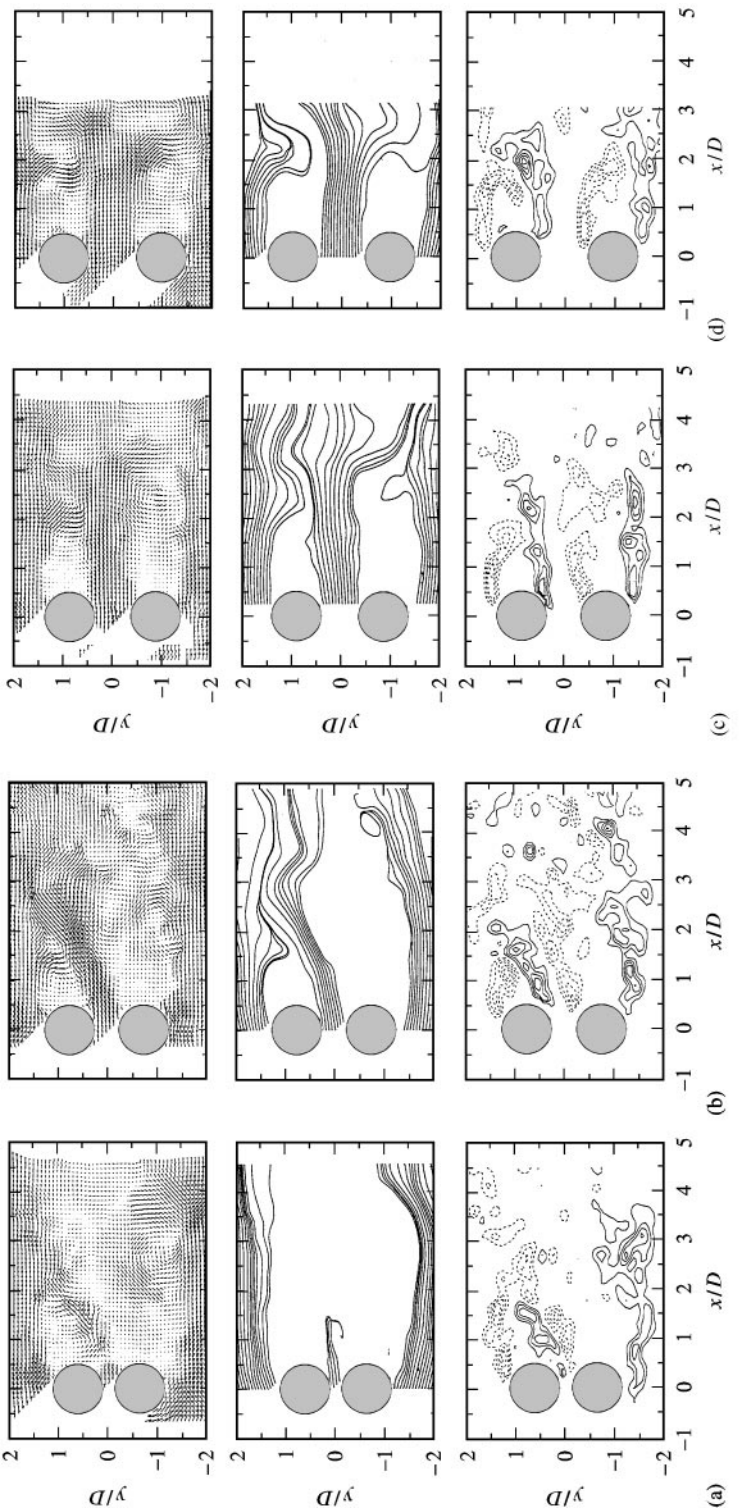

Figure 11. Nondimensional, instantaneous, in-plane velocity, streamline and vorticity fields for two side-by-side circular cylinders of equal diameter in steady cross-flow (from left to right), at intermediate pitch ratio: (a) $T/D = 1{\cdot}25$, Re = 2500; (b) $T/D = 1{\cdot}5$, Re = 1900; (c) $T/D = 1{\cdot}75$, Re = 1900; (d) $T/D = 2{\cdot}0$, Re = 1900. Streamlines arbitrarily chosen. Minimum vorticity contour magnitude of 1·5; vorticity contour magnitude increment of 1·5. Dashed lines represent negative (CW) vorticity.

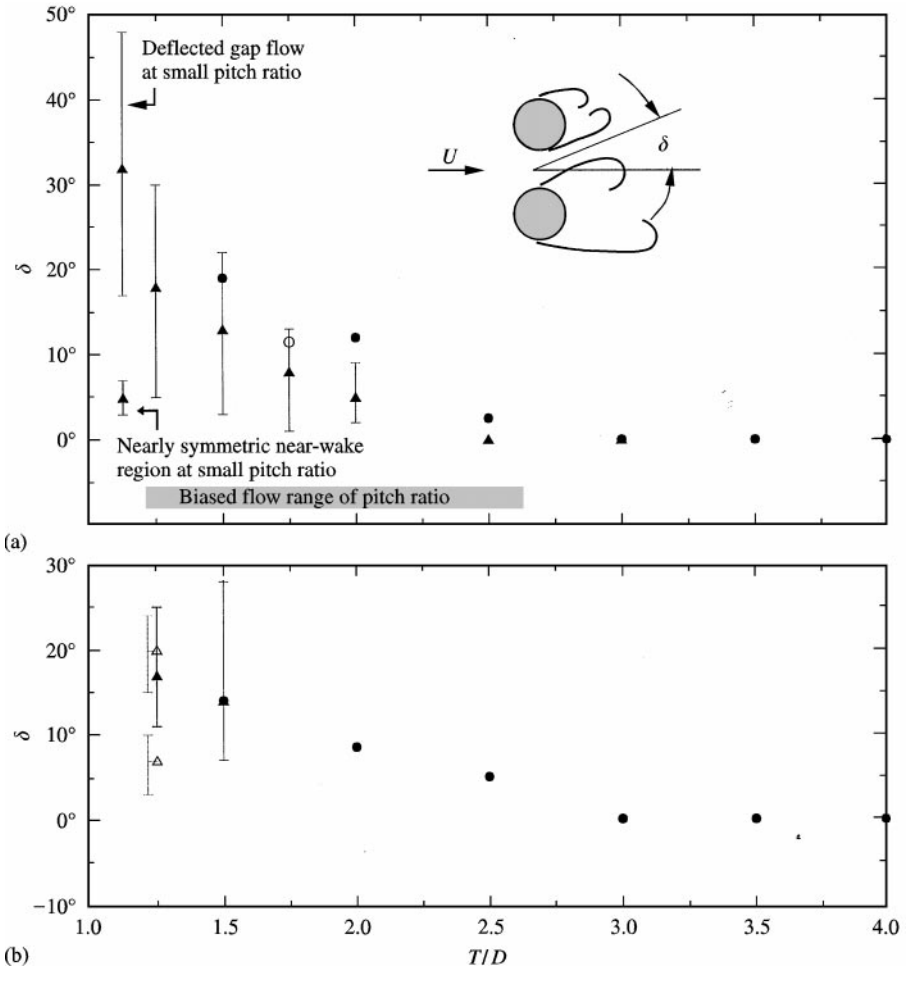

Figure 12. Angle of gap flow deflection, δ, for (a) two and (b) three side-by-side circular cylinders: ●, flow visualization; ▲, PIV; △, asymmetric biased flow pattern, PIV (for three side-by-side cylinders); ○, estimated from Kim & Durbin (1988). Error bars show the range of instantaneous deflection angle from the PIV measurements. The uncertainty is estimated at $\pm 2°$.

only plotted for the mean flow. The streamlines are not plotted in the near-wake regions of the cylinders, since insufficient velocity vector data were present to give realistic streamlines.

Both the flow visualization and PIV results show that the deflection of the biased gap flow varies with T/D. The deflection angle δ (see Figure 12) may be estimated from the flow visualization images and the PIV full-field data, and the data are plotted in Figure 12(a). The trend is toward a smaller degree of deflection with increasing pitch. This trend is similar to the *difference* between the high and low vortex-shedding frequencies at intermediate T/D (corresponding to the biased flow pattern), as shown in Figure 5(a). Although the deflection angles from the flow visualization video images are higher than those seen in the PIV results, this difference may be caused by experimental effects, such as blockage or the cylinder aspect ratio, for example.

Also shown in Figure 12(a) are two values for the deflection angle at $T/D = 1{\cdot}125$, reflecting two of the three flow patterns seen at the small pitch ratio (and previously discussed).

The full-field PIV data also show that the instantaneous deflection angle at a given pitch ratio may itself vary over a wide range, as indicated by the error bars in Figure 12(a). In some cases, the instantaneous deflection of the gap flow is barely detectable, as shown in Figure 11(d) for $T/D = 2{\cdot}0$. A biased flow pattern may still be detected in Figure 11(d), however, since the near-wake region of the upper cylinder appears to be shorter than that of the lower one.

3.3.1. *Vortex dynamics*

In terms of the vortex dynamics of the combined wake for the biased flow pattern, two types of basic behaviour were noted by Williamson (1985) for $\mathrm{Re} \leq 200$. In the first case, vortices formed alongside the biased gap flow are squeezed and amalgamated into the dominant vortices on the outside of the two-cylinder configuration, the side to which the flow is biased. This amalgamation process eventually produces a single vortex street in the combined wake. In the second case, said to be dominant for $T/D = 1{\cdot}6$ to $1{\cdot}9$, the combined wake of the two cylinders is marked by pairs of vortices downstream of the cylinder with the narrow near-wake region, and single larger vortices downstream of the cylinder with the wider near-wake region, on the opposite side. In this case, the gap vortices are amalgamated into the side of the wake where the pairs form. In this study, however, conducted at higher Reynolds number ($\mathrm{Re} = 500$ to 3000) than that of Williamson (1985), neither the flow visualization nor the PIV data clearly demonstrated the existence of either of these two types of basic behaviour. Two reasons may be proposed for this: (i) in the context of the instantaneous vorticity field (from PIV), the vortices become rapidly distorted and lose coherence once they are shed from the cylinders, masking any amalgamation process; and (ii) the amalgamation process may occur further downstream of the cylinders, outside the range of detection of the PIV system used in this study.

The sole form of flow organization observed was anti-phase synchronization [Figure 1(b)] of the two vortex-shedding processes, whereby vortices were formed and shed in a symmetric manner on opposite sides of the deflected gap flow. The synchronization was seen only in the immediate vicinity of the two cylinders, and no established regular pattern of rows of vortices was seen in the combined wake of the two cylinders (as noted in Section 3.4 for large T/D). Such behaviour, under biased flow conditions, would seem to broadly correspond to the "quasiperiodic regime" noted by Peschard & Le Gal (1996).

3.3.2. *Strouhal number data*

The Strouhal number data in Figure 5(a) and the power spectra in Figure 6 show that, within the biased flow range of transverse pitch, two dominant peaks are detected, reflecting the two vortex-shedding frequencies. Although Figure 5(a) shows a range of Strouhal numbers for some pitch ratios, no more than two were detected in a given experiment, and the scatter of the data simply shows that there is some variation in the magnitudes of the two frequencies at a given pitch ratio.

Data from the present study, in Figure 6(d), also show the existence of two dominant frequencies at $T/D = 2{\cdot}5$. The appearance of the two frequencies suggests that the biased flow could exist beyond the traditional biased flow range of $1{\cdot}2 < T/D < 2{\cdot}2$, and indeed a small degree of deflection [recorded in Figure 12(a)] may be seen in the flow visualization images for $T/D = 2{\cdot}5$ [Figure 13(a)]. No apparent deflection is seen in the PIV vorticity data for $T/D = 2{\cdot}5$ (Figure 14), however, and this difference suggests that the detection of multiple frequencies at $T/D = 2{\cdot}5$ might be caused by influences from the experimental

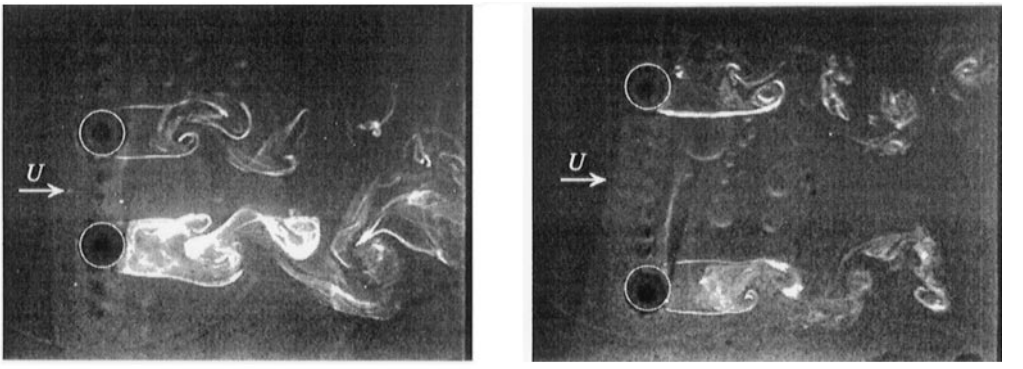

Figure 13. Flow visualization of two side-by-side circular cylinders in steady cross-flow at large T/D, showing anti-phase vortex shedding, for Re = 1000 to 3000: (a) $T/D = 2{\cdot}5$; (b) $T/D = 4{\cdot}5$.

set-up, or possibly result from a transitional behaviour between a predominantly biased flow pattern and a predominantly symmetrical flow pattern.

3.3.3. *Bistable properties*

The biased flow pattern is also known to be bistable (Bearman & Wadcock 1973; Kim & Durbin 1988). The bistable characteristic is not caused by misalignment of the cylinders or other extraneous influences, but is an intrinsic property of the flow; the transverse configuration may be considered to be the transitional arrangement between two staggered configurations of greater and lesser incidence to the incoming flow (Bearman & Wadcock 1973; Kim & Durbin 1988). Peschard & Le Gal (1996), however, who did not observe this bistable behaviour in their low-Reynolds-number water-tunnel experiments, suggest that it may be caused by turbulent perturbations in the incoming flow. In this study, and specifically in the water-tunnel experiments, this bistable nature was not observed either, and the flow remained deflected consistently towards the same cylinder. Only the experiments conducted in the towing tank showed that the near-wakes could be freely deflected towards either of the two cylinders, and this with no changes in alignment or Reynolds number. In the present case, it is suspected that residual motion of the water in the towing tank (i.e. settling of the water after completion of an experiment, or after redistribution of the seeding particles) may be responsible for the selection of the biased flow direction.

3.4. Two Side-by-Side Circular Cylinders with Large T/D

3.4.1. *Vortex-shedding patterns*

At greater pitch ratio, the biased flow disappears, and the side-by-side circular cylinders behave more as independent, isolated bluff bodies. Some interaction or synchronization, however, does occur between the two cylinders. According to Williamson (1985), the predominant fluid behaviour should be one of anti-phase vortex formation and shedding synchronization between the two cylinders, which leads to two parallel vortex streets in the wake [Figure 1(b)]. In the present experiments, anti-phase vortex shedding was noted for the most part, as shown in the flow visualization results in Figure 13 and the PIV results in Figures 14 and 15, although in-phase and irregular shedding processes were also observed

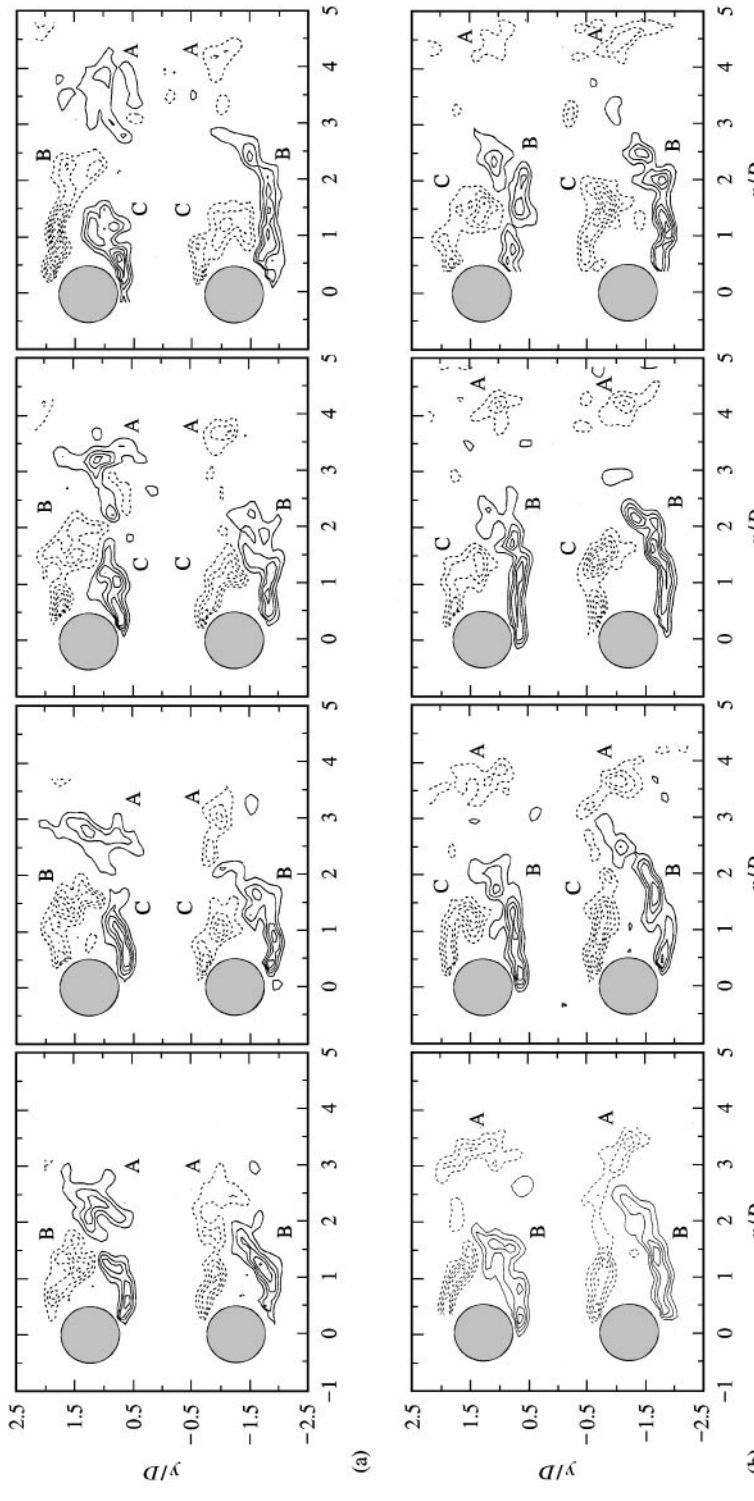

Figure 14. Nondimensional, instantaneous, in-plane vorticity field for two side-by-side circular cylinders of equal diameter in steady cross-flow (from left to right), with $T/D = 2{\cdot}5$, Re = 1900, $\Delta t^* = 0{\cdot}6$, $\Delta t/T_s = 0{\cdot}13$: (a) anti-phase vortex shedding, with corresponding vortices labeled as A, B and C; (b) in-phase vortex shedding, with corresponding vortices labeled as A, B and C. Minimum vorticity contour magnitude of 1·5; vorticity contour magnitude increment of 1·5. Dashed lines represent negative (CW) vorticity.

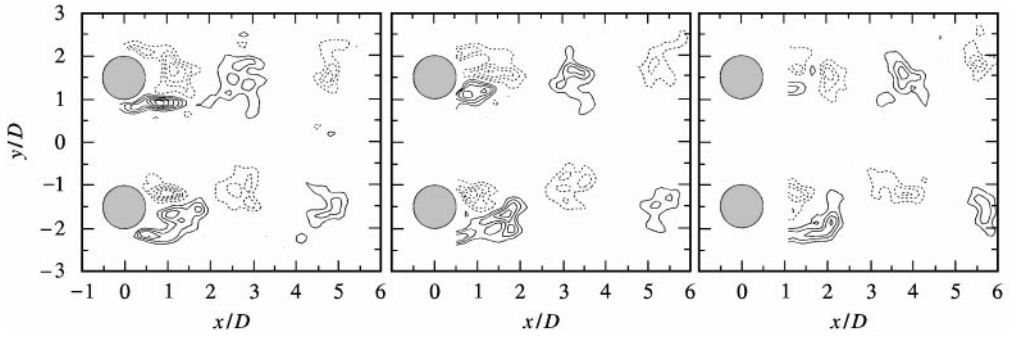

Figure 15. Nondimensional, instantaneous, in-plane vorticity field for two side-by-side circular cylinders of equal diameter in steady cross-flow (from left to right), with $T/D = 3{\cdot}0$, $\mathrm{Re} = 1900$, $\Delta t^* = 0{\cdot}6$, $\Delta t/T_s = 0{\cdot}12$, showing anti-phase vortex shedding synchronization. Minimum vorticity contour magnitude of 1·5; vorticity contour magnitude increment of 1·5. Dashed lines represent negative (CW) vorticity.

[as shown in Figure 14(b)]. The predominance of the anti-phase shedding broadly corresponds to the "Locking Π Phase Opposition" regime noted by Peschard & Le Gal (1996). Although Williamson (1985) indicated that in-phase shedding leads to the formation of a single, binary vortex street in the combined wake of the two cylinders, such a development was not observed in the present PIV experiments. The most likely reason for this is that the combined wake of the two cylinders could not be visualized for sufficient distance downstream with the given PIV system.

The synchronization or interaction of the vortex streets was observed in the water tunnel experiments up to $T/D = 4{\cdot}5$, as shown in Figure 13(b). However, for $T/D > 4{\cdot}5$, any form of synchronization was no longer apparent.

3.4.2. *Vortex strength measurements*

For the $T/D = 3{\cdot}0$ configuration, some measurements of the strength of the shed vortices were obtained from the PIV data and are shown in Figure 16, where the vortex strength is simply the nondimensional circulation Γ/UD. The vortex circulation was found by integrating like-sign vorticity with a magnitude $\omega_z D/U \geq 0{\cdot}75$ over the sub-region of the flow field corresponding to the shed vortex. The vortex centre was defined by the centroid of this region of like-sign vorticity. The measurement uncertainty associated with the vortex strength is estimated at 10%.

The results in Figure 16, and other results obtained for $T/D = 2{\cdot}5$ (not shown), illustrate the decay in strength as the vortex moves further from the body. The vortex strength data in Figure 16 are both for vortices shed alongside the gap and alongside the outer flow. It should be noted that no difference in the decay rates for the inner and outer vortices was noticed, within the limits of experimental uncertainty. This result contrasts with the phase-averaged vorticity measurements of Kolar *et al.* (1997) for two side-by-side square cylinders at $T/D = 3{\cdot}0$, where the strengths of the vortices on either side of the gap were found to decay at a greater rate than those adjacent to the outer flow.

Knowing the streamwise locations of the vortices in each vorticity field, and the time difference between successive fields, the convection velocities of the vortices may be determined. For two circular cylinders at $T/D = 2{\cdot}5$ and 3·0, the convection velocity was estimated at $0{\cdot}84U$ for $2{\cdot}0 < x/D < 6{\cdot}0$. This result compares favourably with $0{\cdot}83U$ for a single circular cylinder as measured by Cantwell & Coles (1983), $0{\cdot}80U$ for two

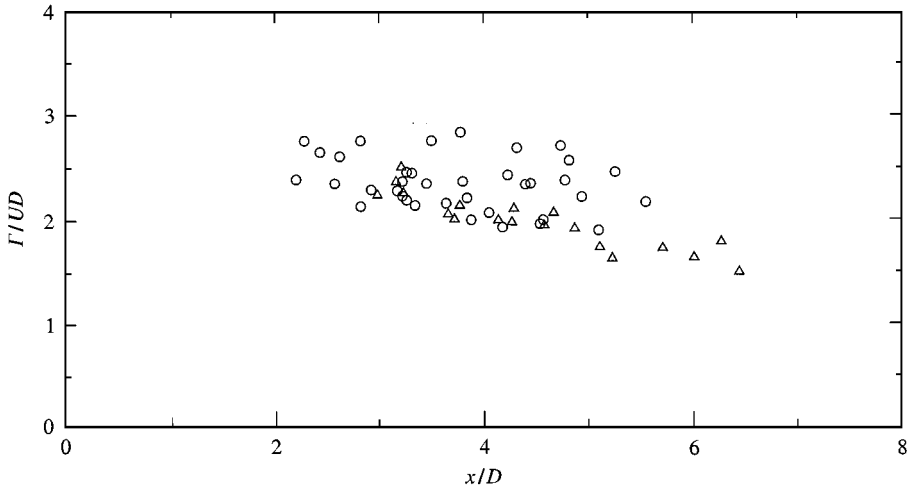

Figure 16. Vortex strength as a function of streamwise distance from the cylinder centre for two side-by-side circular cylinders of equal diameter in steady cross-flow, with $T/D = 3{\cdot}0$, Re = 1900–2500: ○, vortices shed from the gap shear layers; △, vortices shed from the outer shear layers. The limited data represent results from six different PIV experiments, or realizations.

side-by-side circular cylinders as measured by Kim & Durbin (1988), and $0{\cdot}75U$ for two side-by-side square cylinders as measured by Kolar *et al.* (1997). No difference in convection velocity was noticed for the vortices shed alongside the gap, or vortices shed alongside the outer flow, within the limits of experimental uncertainty, similar to that observed by Kolar *et al.* (1997).

3.5. Three Side-by-Side Circular Cylinders with $T/D > 1{\cdot}0$

Kumada *et al.* (1984) indicate the existence of four basic flow patterns for three circular cylinders of equal diameter arranged side-by-side: (i) single bluff-body behaviour for $T/D < 1{\cdot}125$, in which a single vortex street forms in the combined wake of the three cylinders; (ii) asymmetric biased flow for $1{\cdot}125 < T/D < 1{\cdot}35$, in which one of the outer cylinders has a large near-wake region compared to that of the central cylinder and the opposite outer cylinder, and both gap flows are biased away from the large near-wake region; (iii) symmetric biased flow for $1{\cdot}35 < T/D < 2{\cdot}2$, in which a large near-wake region is found behind the central cylinder, and the gap flows are biased towards the outer cylinders, which themselves have smaller near-wake regions of higher (but equal) shedding frequency; and (iv) synchronized, unbiased vortex shedding of the same frequency from each cylinder for $T/D > 2{\cdot}2$. Two of these flow patterns may be seen in the flow visualization results shown in Figure 17, with symmetric biased flow for $T/D = 1{\cdot}5$ and $2{\cdot}0$ shown in Figure 17(a, b), and synchronized unbiased vortex shedding for $T/D = 2{\cdot}5$ and $3{\cdot}0$ shown in Figure 17(c, d). Vortex shedding observed in the latter two cases, [Figure 17(c, d)] occurs in the anti-phase fashion across the two gaps, similar to that observed for two-cylinders.

3.5.1. *Vortex shedding frequencies*

Measurements of the vortex shedding frequencies from this study, shown previously in Figure 5(b), support the existence of these two flow patterns and compare favourably with

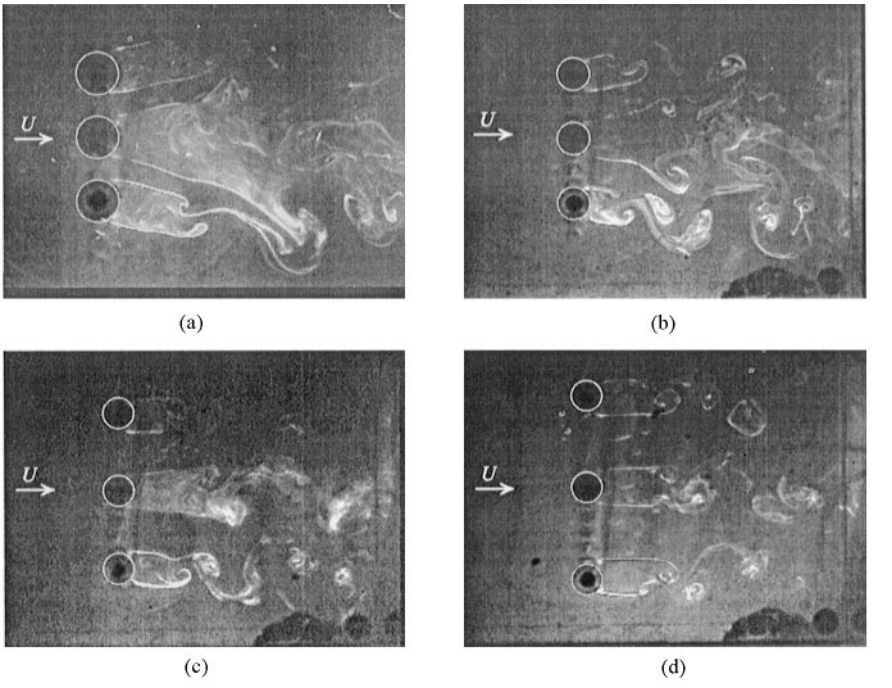

Figure 17. Flow visualization of three side-by-side circular cylinders in steady cross-flow at Re = 1000 to 3000: (a) $T/D = 1{\cdot}5$; (b) $T/D = 2{\cdot}0$; (c) $T/D = 2{\cdot}5$; (d) $T/D = 3{\cdot}0$. Symmetric biased flow patterns are shown for $T/D = 1{\cdot}5$, 2·0, and 2·5. The biased flow at $T/D = 2{\cdot}5$ [in (c)] extends the T/D range for this flow pattern, and is consistent with the detection of a range of frequencies at this pitch ratio, as shown in Figure 5(b).

previously published results, with a single Strouhal number detected for $T/D > 2{\cdot}5$, and two Strouhal numbers for $1{\cdot}5 \leq T/D \leq 2{\cdot}5$. The published data also show a third, intermediate frequency for $1{\cdot}0 < T/D < 1{\cdot}5$ that likely corresponds to the asymmetric biased flow pattern [see Figure 20(a)]; in this study, however, Strouhal number measurements were not done for three-cylinder configurations in this range of pitch ratio.

Both the published data and results from this study show a pair of high frequencies at $T/D = 1{\cdot}5$. These results suggest that the structure of the wake is more complex than that revealed in the flow visualization. In Figure 18, power spectra for the $T/D = 1{\cdot}5$ configuration are plotted for a range of streamwise x/D and cross-stream y/D locations. Low-frequency shedding from the wider near-wake region of the central cylinder, at St = 0·05–0·06, is detected at all x/D and y/D locations. This lower frequency can also be determined by counting vortices on the video frames. The higher frequency of vortex shedding at St = 0·31–0·33, associated with shedding from both outer cylinders, is also found at each x/D and y/D location. This frequency too can be confirmed from the flow visualization video. In Figure 18(e, f), however, a second high-frequency peak (as cited at the beginning of the paragraph) of St = 0·27–0·28 is also found. By inspection, this frequency appears to be a difference between the first two shedding frequencies. Since this third frequency is found only at $x/D = 3{\cdot}0$ and for $y/D > 1{\cdot}5$, it would appear to be associated with pairing of the high- and low-frequency vortices in the combined wake of the three cylinders away from the immediate near-wake regions.

For the two-cylinder configurations discussed earlier, the number of shedding frequencies detected was not highly sensitive to the measurement location.

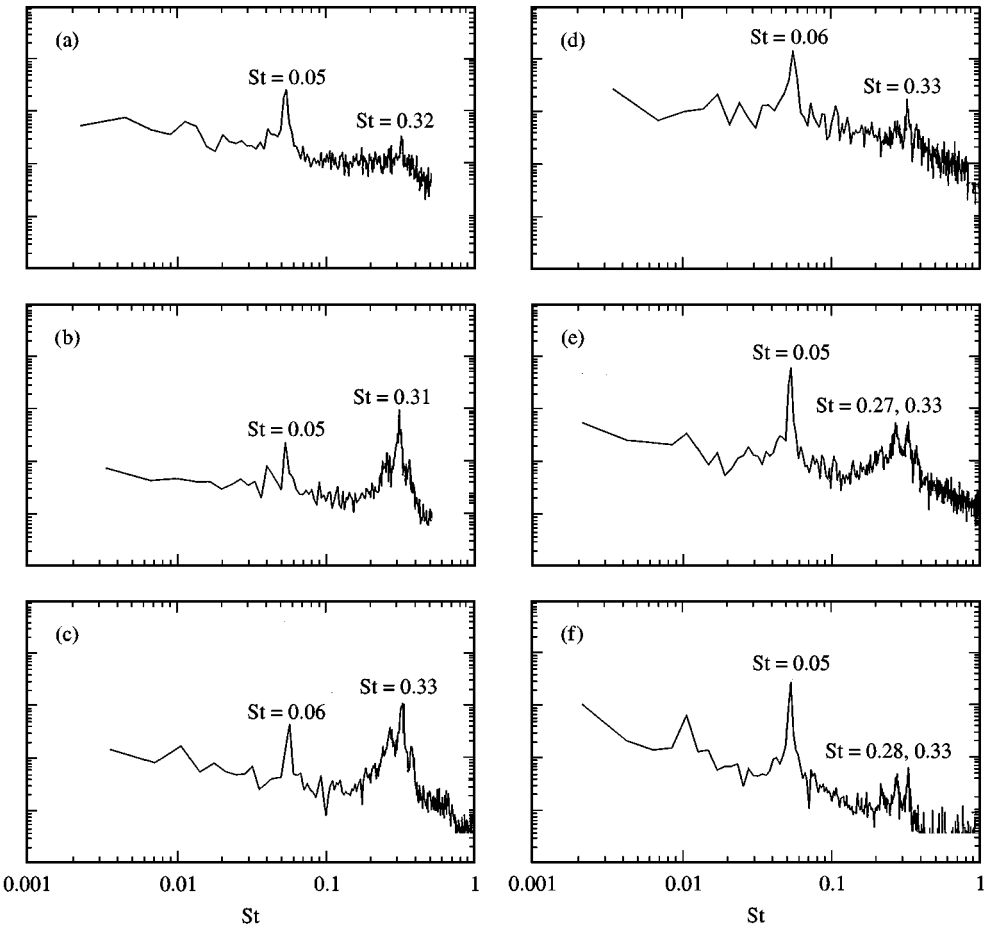

Figure 18. Representative power spectra for three side-by-side circular cylinders in steady cross-flow, with $T/D = 1{\cdot}5$: (a) $x/D = 2{\cdot}0$, $y/D = 2{\cdot}0$, Re = 1750; (b) $x/D = 2{\cdot}0$, $y/D = 2{\cdot}5$, Re = 1200; (c) $x/D = 2{\cdot}0$, $y/D = 3{\cdot}0$, Re = 1100; (d) $x/D = 3{\cdot}0$, $y/D = 1{\cdot}5$, Re = 1100; (e) $x/D = 3{\cdot}0$, $y/D = 2{\cdot}5$, Re = 1800; (f) $x/D = 3{\cdot}0$, $y/D = 3{\cdot}5$, Re = 1800. Vertical scale is arbitrary, but the same for each spectrum.

3.5.2. *Flow patterns*

The PIV results for $T/D = 1{\cdot}125$, $1{\cdot}25$, and $1{\cdot}5$ (Figures 19, 20 and 21, respectively) support the existence of the first three flow patterns: those of the single bluff-body behaviour, and the asymmetric and symmetric biased flows. The pitch ratio boundaries for these flow patterns were found to differ somewhat from those proposed by Kumada *et al.* (1984), however, and some variation in the flow structure was noted at each T/D tested. The deflection angles of the two gap flows estimated from the flow visualization and PIV results are shown in Figure 12(b).

At $T/D = 1{\cdot}125$ (Figure 19), a single vortex street forms in the combined wake of the three cylinders, similar to that of a single bluff-body. Although weak, the gap flow is apparent, and shows a preferential bias towards the vortex being formed [similar to two cylinders at $T/D = 1{\cdot}125$, shown in Figure 9(b)]. The deflection angle was difficult to determine precisely from the PIV data, and hence it is not presented in Figure 12(b).

At $T/D = 1{\cdot}25$ (Figure 20), both the asymmetric and symmetric biased flow patterns were found, although the latter was more commonly observed. The asymmetric biased flow,

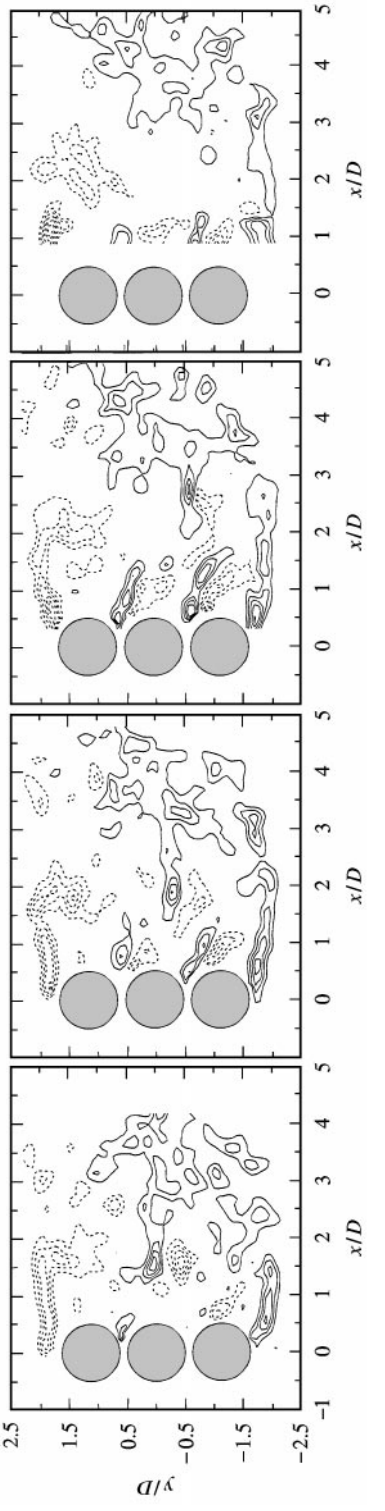

Figure 19. Nondimensional, instantaneous, in-plane vorticity field for three side-by-side circular cylinders of equal diameter in steady cross-flow (from left to right), with $T/D = 1{\cdot}125$, $\mathrm{Re} = 1900$, $\Delta t^* = 0{\cdot}6$, $\Delta t/T_s = 0{\cdot}04$. Minimum vorticity contour magnitude of 1·5; vorticity contour magnitude increment of 1·5. Dashed lines represent negative (CW) vorticity.

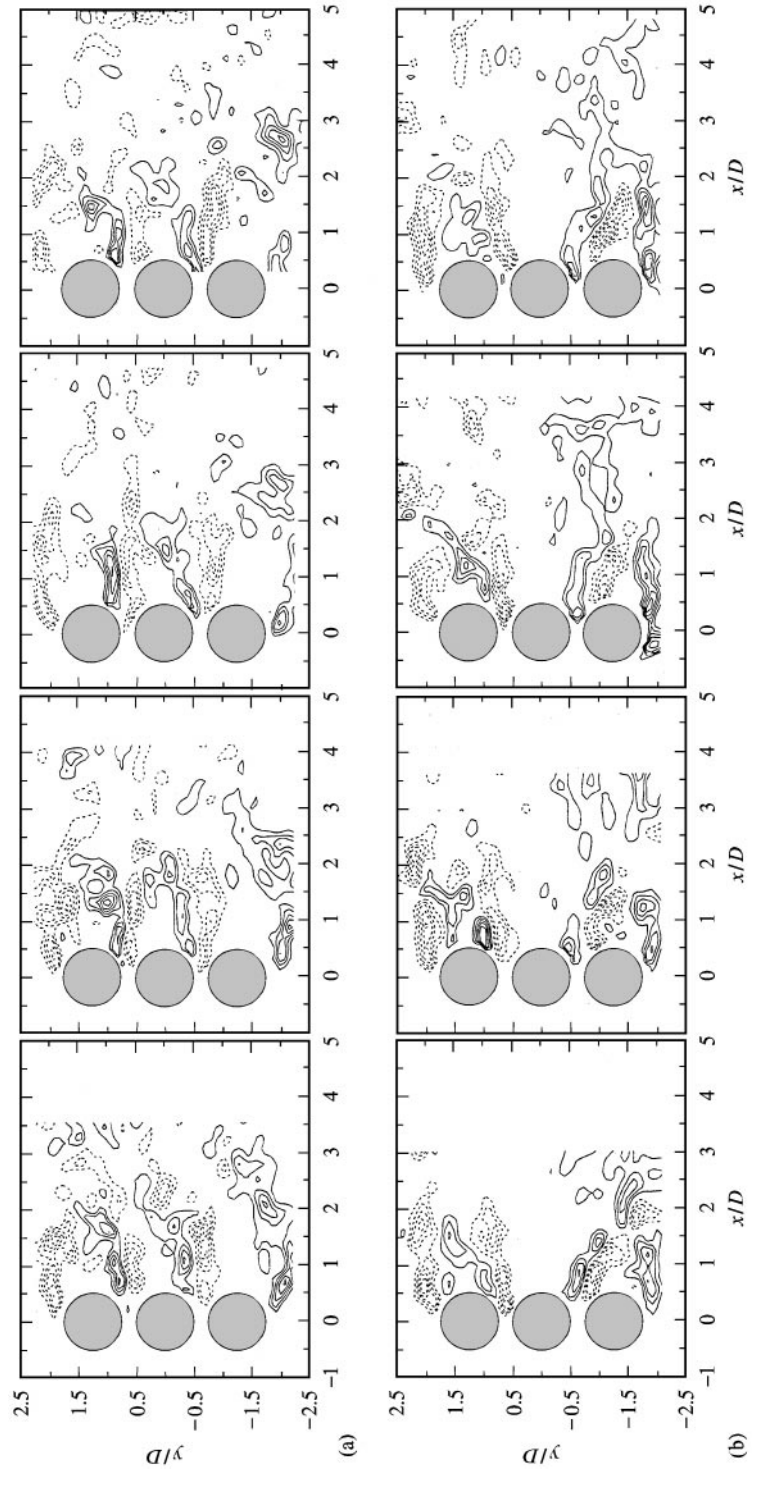

Figure 20. Nondimensional, instantaneous, in-plane vorticity field for three side-by-side circular cylinders of equal diameter in steady cross-flow (from left to right), with $T/D = 1{\cdot}25$: (a) asymmetric biased flow pattern, with wide near-wake behind the lower cylinder, Re = 1900, $\Delta t^* = 0{\cdot}6$, and $\Delta t/T_s = 0{\cdot}05$ or $0{\cdot}14$, based on low and high vortex shedding frequencies, respectively; (b) symmetric biased flow pattern, Re = 1900, $\Delta t^* = 0{\cdot}6$, $\Delta t/T_s = 0{\cdot}05$ or $0{\cdot}14$; (c) asymmetric biased flow pattern, with wide wake behind the lower cylinder, Re = 2500, $\Delta t^* = 0{\cdot}8$, $\Delta t/T_s = 0{\cdot}06$ or $0{\cdot}19$; (d) nearly-symmetric biased flow pattern, Re = 2900, $\Delta t^* = 0{\cdot}8$, $\Delta t/T_s = 0{\cdot}06$ or $0{\cdot}19$. Minimum vorticity contour magnitude of 1·5; vorticity contour magnitude increment of 1·5. Dashed lines represent negative (CW) vorticity.

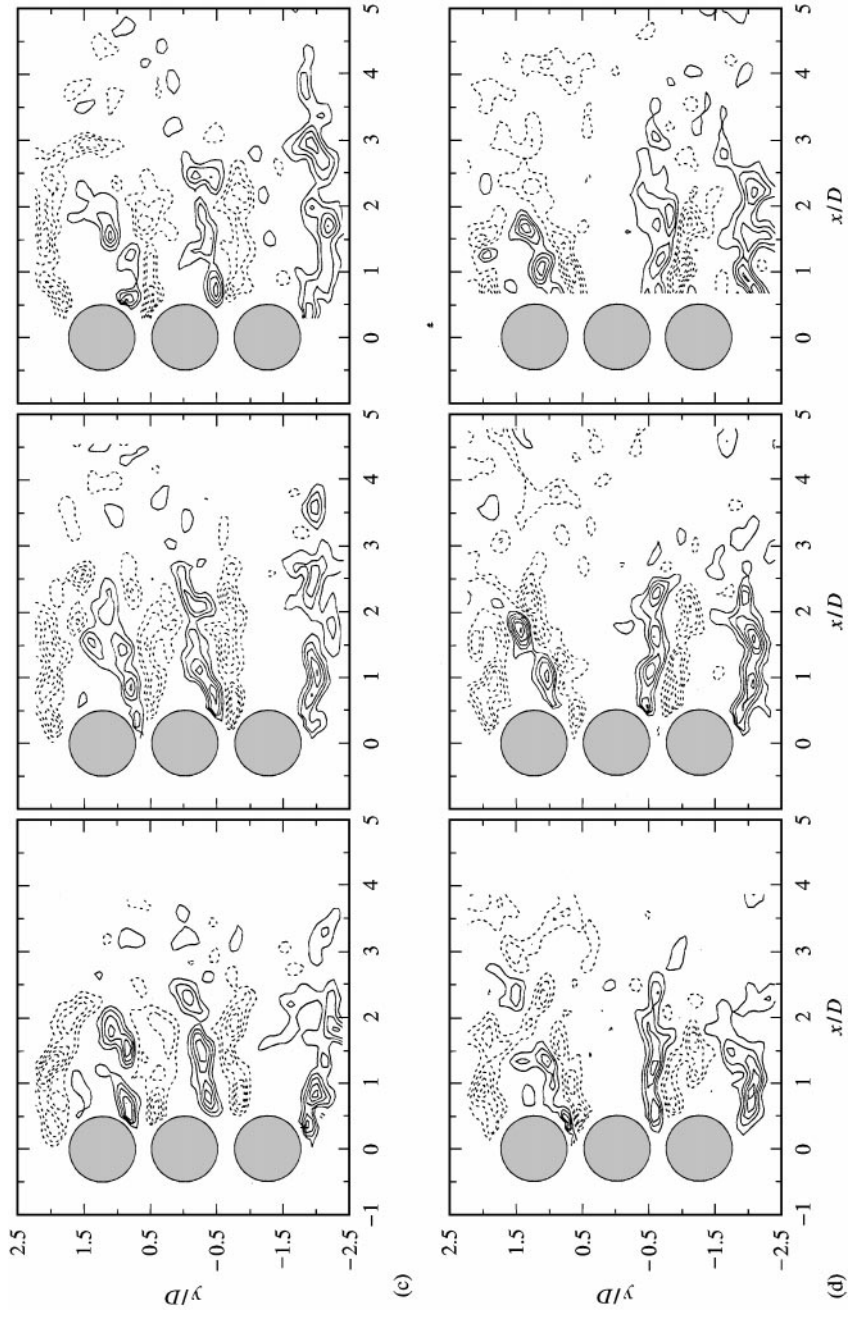

Figure 20. *Continued.*

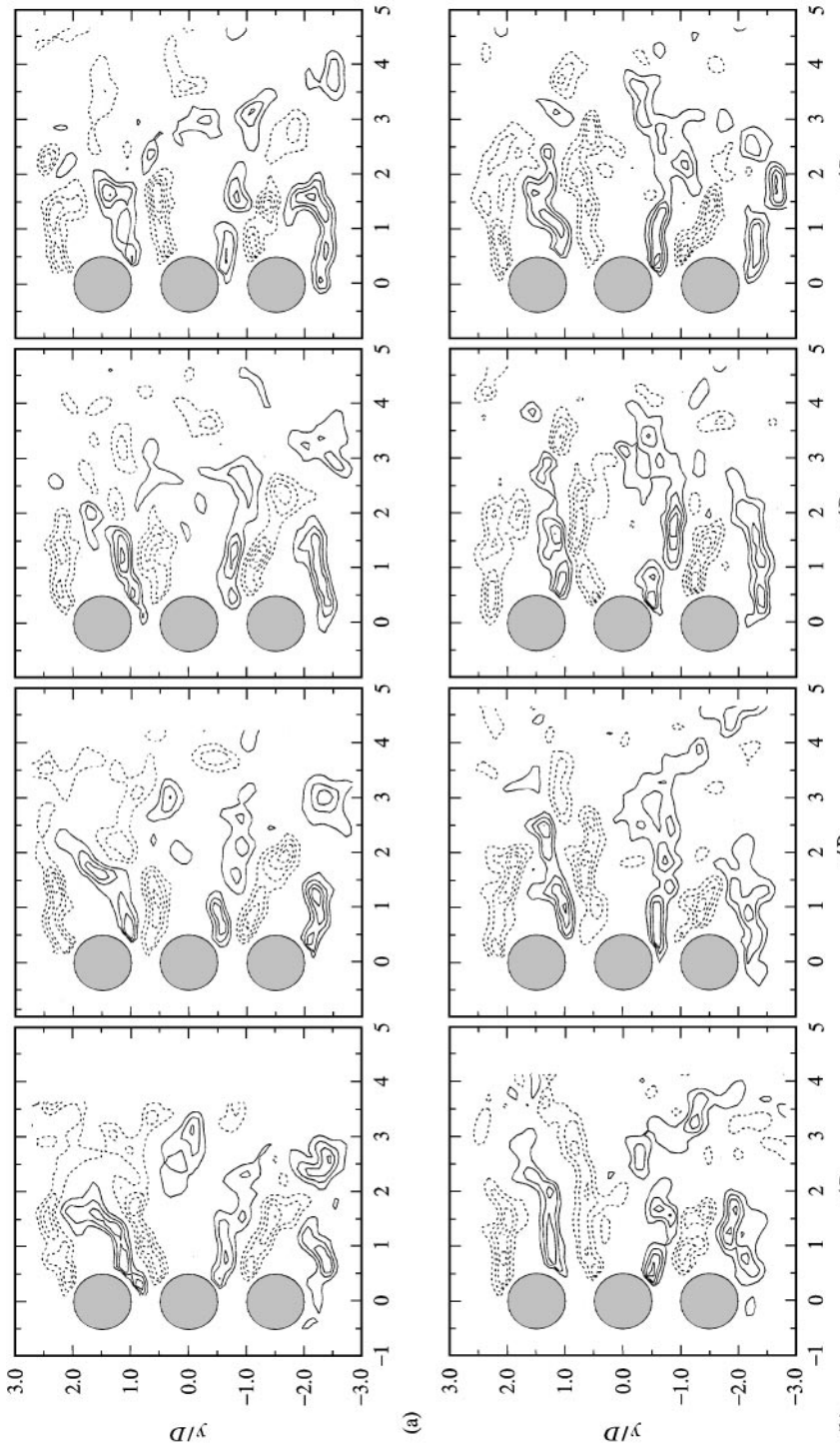

Figure 21. Nondimensional, instantaneous, in-plane vorticity field for three side-by-side circular cylinders of equal diameter in steady cross-flow (from left to right), with $T/D = 1{\cdot}5$: (a) and (b) $\mathrm{Re} = 1900$, $\Delta t^* = 0{\cdot}6$, $\Delta t/T_s = 0{\cdot}04$ or $0{\cdot}22$ based on low or high vortex-shedding frequencies respectively. Minimum vorticity contour magnitude of 1·5; vorticity contour magnitude increment of 1·5. Dashed lines represent negative (CW) vorticity.

shown in Figure 20(a, c), may result in a single vortex street similar to single bluff-body flow, or it may represent one phase of an alternating flow pattern in which the flow is biased first to one of the outer cylinders and then to the other. In either case, two different deflection angles may be noted, one for each gap, as shown in Figure 12(b). Otherwise, the flow may be biased in a stable manner to one of the outer cylinders, with a nearly identical deflection angle for the two gap flows [although it varies over the range shown within the error bars in Figure 12(b)]. The symmetric biased flow, shown in Figure 20(b, d), results in a more complex combined wake region. This temporal variation in the flow pattern at a given T/D and Re may account for the additional frequency signals noted for three cylinders in Figure 5(b), for $1{\cdot}0 < T/D < 1{\cdot}5$.

Finally, at $T/D = 1{\cdot}5$, only the symmetric biased flow pattern is observed (Figure 21). The instantaneous deflection angle is again nearly identical for the two gap flows, but can vary over a wide range [as shown in Figure 12(b)].

4. CONCLUSIONS

This study represents a detailed investigation of the wake flows behind two and three circular cylinders of equal diameter arranged in side-by-side configurations and immersed in steady cross-flow in the lower subcritical Reynolds number range, for Re = 500–3000. Three experimental techniques, flow visualization, hot-flim anemometry, and particle image velocimetry (PIV), were used to obtain an understanding of the fluid behaviour for two- and three-cylinder arrangements of different transverse pitch ratio T/D. For the range of Reynolds number for which this study was conducted, virtually no variation in measured quantities or differences in the flow patterns were noted, and the results were in most cases similar to those observed at both lower and higher Reynolds numbers by other researchers. This finding lends further support to the essential Reynolds number independence of this arrangement of circular cylinders.

For the two-cylinder arrangements, the three basic flow patterns of single bluff-body vortex shedding at small T/D, biased flow at intermediate T/D, and synchronized vortex shedding at larger T/D, were confirmed. The PIV results showed the range of pitch ratio for the biased flow pattern to extend from $1{\cdot}25 \leq T/D \leq 2{\cdot}0$, although vortex shedding frequency measurements obtained from hot-film anemometry indicated the presence of two frequencies also at $T/D = 2{\cdot}5$. The reported bistable nature of the biased flow was not detected in the water tunnel experiments. This may be attributable to a combination of (i) a small degree of misalignment of the cylinders, and (ii) experimental effects such as aspect ratio and blockage. It is noted that previous experiments in which the bistable flow pattern was reported (Bearman & Wadcock 1973; Kim & Durbin 1988) were conducted only in wind tunnels [Table 1(a)]; whether this is a coincidence or there is a deeper underlying reason is presently unknown.

For the three-cylinder arrangements, either single bluff-body behaviour or an asymmetric biased flow pattern could be observed at small T/D, whereas a symmetric biased flow pattern was found at intermediate T/D. The PIV experiments in particular provide some detailed insight into the fluid dynamics of this cylinder configuration.

For both the two- and three-cylinder arrangements, the use of PIV to obtain instantaneous representations of the in-plane vorticity field revealed considerable variation in the reported flow patterns at a given T/D (not related to varying Re). Variations were noted in the streamwise location of vortex formation, the angle of deflection of biased gap flow, and in the synchronization of vortex-shedding processes. It is suggested that some of this variation may explain the detection of more than two dominant frequencies in the flow field for three side-by-side circular cylinders with $1{\cdot}0 < T/D < 1{\cdot}5$.

ACKNOWLEDGEMENTS

The authors would like to acknowledge the financial support of the Natural Sciences and Engineering Research Council (NSERC) of Canada, and Les Fonds pour la Formation de Chercheurs et l'Aide à la Recherche (FCAR) of the Province of Québec.

References

Bearman, P. W. & Wadcock, A. J. 1973 The interaction between a pair of circular cylinders normal to a stream. *Journal of Fluid Mechanics* **61,** 499–511.

Cantwell, B. & Coles, D. 1983 An experimental study of entrainment and transport in the turbulent near wake of a circular cylinder. *Journal of Fluid Mechanics* **136,** 321–374.

Cheng, M. & Moretti, P. M. 1988 Experimental study of the flow field downstream of a single tube row. *Experimental Thermal and Fluid Science* **1,** 69–74.

Chyu, C.-K. & Rockwell, D. 1996 Kármán vortex development: relation to symmetry and circulation of transition vortices. *AIAA Journal* **34,** 1954–1956.

Eastop, T. D. & Turner, J. R. 1982 Air flow around three cylinders at various pitch-to-diameter ratios for both a longitudinal and a transverse arrangement. *Transactions of the Institution of Chemical Engineers* **60,** 359–363.

Hori, E. 1959 Experiments on flow around a pair of parallel circular cylinders. *Proceedings of the* 9*th Japan National congress for Applied Mechanics*, paper III-11, pp. 231–234.

Ishigai, S. & Nishikawa, E. 1975 Experimental study of structure of gas flow in tube banks with tube axes normal to flow (Part II, On the structure of gas flow in single-column, single-row, and double-row tube banks). *Bulletin of the JSME* **18,** 528–535.

Ishigai, S., Nishikawa, E., Nishimura, K. & Cho, K. 1972 Experimental study of structure of gas flow in tube banks with tube axes normal to flow (Part I, Kármán vortex flow from two tubes at various spacings). *Bulletin of the JSME* **15,** 949–956.

Jendrzejczyk, J. A. & Chen, S. S. 1986 Fluid forces on two circular cylinders in cross-flow. In *Flow-Induced Vibration — 1986*: (eds S. S. Chen, J. C. Simonis & Y. S. Shin), Chicago, IL, PVP-Vol. 104, pp. 1–13. New York: ASME.

Kamemoto, K. 1976 Formation and interaction of two parallel vortex streets. *Bulletin of the JSME* **19,** 283–290.

Kim, H. J. & Durbin, P. A. 1988 Investigation of the flow between a pair of circular cylinders in the flopping regime. *Journal of Fluid Mechanics* **196,** 431–448.

Kiya, M., Arie, M., Tamura, H. & Mori, H. 1980 Vortex shedding from two circular cylinders in staggered arrangement. *ASME Journal of Fluids Engineering* **102,** 166–173.

Kolar, V., Lyn, D. A. & Rodi, W. 1997 Ensemble-averaged measurements in the turbulent near wake of two side-by-side square cylinders. *Journal of Fluid Mechanics* **346,** 201–237.

Kumada, M., Hiwada, M., Ito, M. & Mabuchi, I. 1984 Wake interference between three circular cylinders arranged side-by-side normal to a flow. *Transactions of the JSME* **50,** 1699–1707 (in Japanese).

Kwon, S. H., Park, J., Ha, D. D. & Lee, Y. H. 1996 Experimental study of flow fields around cylinder arrays using PIV. *Proceedings of the Sixth International Offshore and Polar Engineering Conference*, Vol. III, pp. 145–150, Los Angeles, U.S.A., May 26–31, 1996.

Le Gal, P., Chauve, M. P., Lima, R. & Rezende, J. 1990 Coupled wakes behind two circular cylinders. *Physical Review A* **41,** 4566–4569.

Le Gal, P., Peschard, I., Chauve, M. P. & Takeda, Y. 1996 Collective behaviour of wakes downstream of a row of cylinders. *Physics of Fluids* **8,** 2097–2106.

Moretti, P. M. & Cheng, M. 1987 Instability of flow through tube rows. *ASME Journal of Fluids Engineering* **109,** 197–198.

Peschard, I. & Le Gal, P. 1996 Coupled wakes of cylinders. *Physical Review Letters* **77,** 3122–3125.

Spivack, H. M. 1946 Vortex frequency and flow pattern in the wake of two parallel cylinders at varied spacing normal to an air stream. *Journal of the Aeronautical Sciences* **13,** 289–297.

Sumner, D., Wong, S., Price, S. J. & Païdoussis, M. P. 1997 Two and three side-by-side circular cylinders in steady cross-flow. *Proceedings of the* 16*th Canadian Congress of Applied Mechanics*, Vol. 1, pp. 273–274.

Szepessy, S. 1993 On the control of circular cylinder flow by end plates. *European Journal of Mechanics B/Fluids* **12,** 217–244.

Wei, T. & Smith, C. R. 1986 Secondary vortices in the wake of circular cylinders. *Journal of Fluid Mechanics* **169,** 513–533.
Willert, C. E. & Gharib, M. 1991 Digital particle image velocimetry. *Experiments in Fluids* **10,** 181–193.
Williamson, C. H. K. 1985 Evolution of a single wake behind a pair of bluff bodies. *Journal of Fluid Mechanics* **159,** 1–18.
Zdravkovich, M. M. & Pridden, D. L. 1977 Interference between two circular cylinders; series of unexpected discontinuities. *Journal of Industrial Aerodynamics* **2,** 255–270.
Zdravkovich, M. M. & Stonebanks, K. L. 1990 Intrinsically nonuniform and metastable flow in and behind tube arrays. *Journal of Fluids and Structures* **4,** 305–319.

APPENDIX: NOMENCLATURE

D	cylinder diameter (mm)
f_s	vortex shedding frequency (Hz)
Re	Reynolds number, based on cylinder diameter and cross-flow velocity
St	Strouhal number, based on cylinder diameter and cross-flow velocity
T	centre-to-centre transverse pitch (mm)
T_s	vortex shedding period (s)
Δt	time interval between sets of vorticity data (s)
Δt^*	nondimensional time interval between sets of vorticity data
$\Delta t/T_s$	time interval as a fraction of the vortex-shedding period
T/D	transverse pitch ratio
U	steady cross-flow velocity (mm/s)
x	streamwise coordinate (mm)
y	cross-stream or transverse coordinate (mm)
Γ	circulation of vortex strength (mm^2/s)
Γ/UD	nondimensional vortex strength
δ	deflection angle (deg)
ω_z	in-plane vorticity (s^{-1})